High Efficiency Single Crystal CdTe Solar Cells

November 19, 2009 — January 31, 2011

Michael Carmody and Angelo Gilmore
EPIR Technologies
Bolingbrook, Illinois

High Efficiency Single Crystal CdTe Solar Cells

November 19, 2009 — January 31, 2011

Michael Carmody and Angelo Gilmore
EPIR Technologies
Bolingbrook, Illinois

NREL Technical Monitor: Brian Keyes
Prepared under Subcontract No. NEU-0-99010-12

National Renewable Energy Laboratory
1617 Cole Boulevard
Golden, Colorado 80401
303-275-3000 • www.nrel.gov

Table of Contents

List of Figures

List of Tables

1 Overview

The goal of the program was to develop single crystal CdTe-based top cells grown on Si solar cells as a platform for the subsequent manufacture of high efficiency tandem cells for CPV applications. The program goal architecture, a single-junction single-crystal CdTe-based solar cell grown epitaxially on an inactive p-type doped Si substrate, is shown on the left in Figure 1. EPIR's tandem cell architecture that is currently under development (not as a part of this program) is shown on the right in Figure 1. The keys to both the single junction and the tandem junction cell architectures are the ability to grow high quality single-crystal CdTe and CdZnTe layers on p-type Si substrates, to dope the CdTe and CdZnTe controllably, both n and p-type, and to make low resistance ohmic front and back contacts.
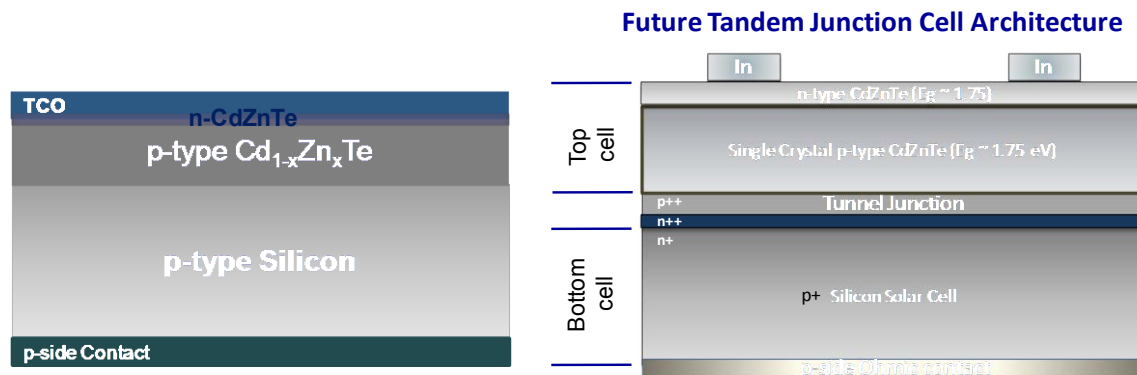
Figure 1. Preincubator program cell architecture (left) and EPIR's future tandem cell architecture that is currently under development (right).

The specific goals of the program were as follows:

1. MBE growth and delivery of single-crystal epitaxial CdTe/Si with an X-ray double-crystal rocking curve full-width-at-half-maximum (DCRC FWHM) < 200 arcsec and of single-crystal epitaxial CdZnTe/Si with sufficiently good crystallinity for the fabrication of high efficiency solar cells (minority carrier recombination lifetimes 100 ns or longer for unintentionally doped samples),

2. N-type doping and delivery of CdTe/Si or CdZnTe/Si with $n > 3 \times 10^{16}$,

3. P-type doping and delivery of CdTe/Si or CdZnTe/Si with $p > 3 \times 10^{15}$,

4. Achievement and delivery of an extrinsically p-doped CdTe/Si or CdZnTe/Si sample with a minority carrier lifetime $\tau \geq 100$ ns, and

5. Fabrication and delivery of a single-junction CdTe/Si or CdZnTe/Si solar cell with efficiency $\eta \geq 15\%$ (dropped from contract).

EPIR Technologies, Inc. (hereinafter EPIR) met and, in terms of the numbers obtained for the FWHM, doping levels and lifetime, substantially exceeded the first four of these goals. Early in the program EPIR also fabricated a single-junction epitaxial CdZnTe solar cell grown on p-type Si having an efficiency measured in-house to be $\eta = 16.4\%$ and almost certainly meeting the

efficiency requirement of the fifth goal. However, this cell was inadvertently destroyed during further experimentation. We were unable to reproduce the doping achieved in that cell and as a result have had non-ohmic blocking contacts. Thus, we were not able to deliver a cell meeting the fifth goal. We are now engaged in a systematic and methodical experimental study of all of the issues involved in doping and contacting n- and p-type CdTe and CdZnTe, are making steady progress and are confident of solving those issues and reproducibly fabricating CdZnTe cells with efficiencies $\eta \geq 20\%$.

Because CdTe solar cells have an almost ideal bandgap for single-junction solar cells, we initially proposed goals for our Preincubator program solely for CdTe/Si and CdTe single-junction solar cells. However, although single-junction CdZnTe cells with a 1.8 eV bandgap have a substantially smaller theoretical efficiency than single-junction CdTe cells, that bandgap is ideal for two-junction cells with a Si bottom junction. For that reason, such CdZnTe cells are more relevant to the EPIR goal of obtaining multijunction cells consisting of II-VI top junctions grown on Si bottom junctions. Therefore, in consultation with NREL and the Department of Energy, we redirected our research toward the obtaining of high efficiency CdZnTe solar cells with a 1.8 eV bandgap, rather than high efficiency CdTe cells.

2   Focus of the First Quarter (Q1)

EPIR's focus during the first quarter was to fulfill the Q1 objectives in the Preincubator proposal. The key technology developments targeted during Q1 of the program were as follows:

1. Establish the growth of thin-film single crystal CdTe (111) on Si substrates using molecular beam epitaxy (MBE) with an x-ray Double Crystal Rocking Curve (DCRC) FWHM < 200 arcsec.

2. Achieve CdTe n-type doping with a carrier concentration $> 3 \times 10^{16}$ cm^{-3}.

3. Achieve CdTe p-type doping with a carrier concentration $> 3 \times 10^{15}$ cm^{-3}.

4. Develop a low resistance ohmic contact to n-type CdTe.

2.1   Growth of Thin-Film Single-Crystal CdTe (111) on Si

Single-crystal CdTe is grown epitaxially by MBE on (111) oriented Si substrates at EPIR. The quality of the single crystal CdTe film is typically measured by x-ray diffraction and is reported as a double-crystal rocking curve full-width-at-half–maximum (DCRC FWHM). Figure 2 is a plot of the DCRC FWHM of recent single-crystal CdTe/Si layers grown at EPIR. A typical MBE grown CdTe/Si layer has a rocking curve FWHM < 200 arcsec. The thickness of these layers varies from 5 – 12 μm.
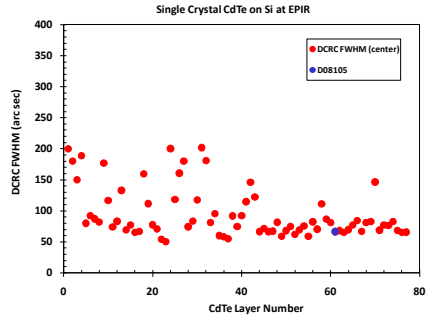
Figure 2. DCRC FWHM of recent single crystal CdTe on Si growths at EPIR. The measurement is from the center of the wafer. The blue icon represents the sample delivered to NREL as part of the Preincubator program.

Figure 3 shows a DCRC FWHM mapping and a representative single diffraction peak from layer D08105, which was sent to NREL for verification as part of the Preincubator program deliverable for Q1.
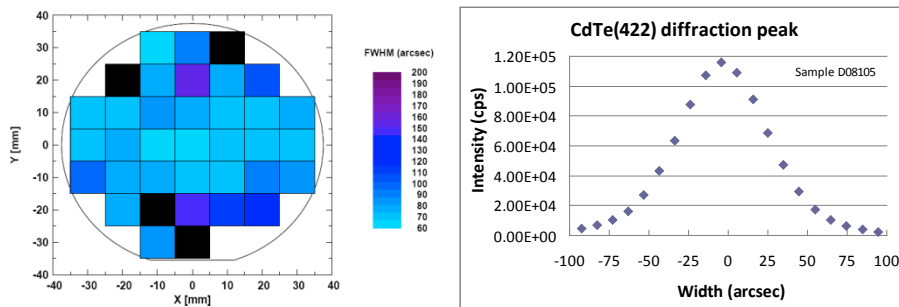
Figure 3. DCRC FWHM map and representative single rocking curve diffraction peak from CdTe/Si layer D08105.

2.2   Establish CdTe n-type Doping with a Carrier Concentration > 3 x 10^{16} cm^{-3}

CdTe was grown on highly resistive (211)-oriented Si substrates for Hall measurement purposes and on highly conductive (111) oriented p-type Si substrates (Si resistivity ~ 0.009 Ω-cm) to extract the carrier concentration from C-V measurements. The CdTe samples were undoped in the "as-grown" state. The average layer DCRC FWHM of these films varied between 100 and 160 arcsec.

2.2.1 Sample Preparation

The CdTe samples were doped n-type by post-growth diffusion of indium into the sample from the top surface of the CdTe film. The CdTe surface was cleaned and etched with a DI water/HCl solution prior to loading the sample into the evaporation chamber. E-beam evaporation was used to deposit In on the freshly etched CdTe surface. The Hall samples were annealed using Rapid Thermal Annealing (RTP) in a nitrogen ambient. The longer annealing time was used to diffuse

7

the indium to the back surface of the CdTe, resulting in a relatively uniform and flat indium profile across the CdTe film to the CdTe/Si interface (see Figure 4). After the diffusion anneal, the excess In was etched off the sample surface using an HCl solution. A thick Al layer was deposited on the back surface of the Si and annealed to establish an ohmic contact to the p-type Si substrate for the C-V analysis.

Indium tin oxide (ITO) was used to establish good ohmic contact to the indium-diffused n-type CdTe. The ITO was patterned using photolithography and selectively removed, leaving behind only contact pads for van der Pauw Hall measurements (see Figure 5).
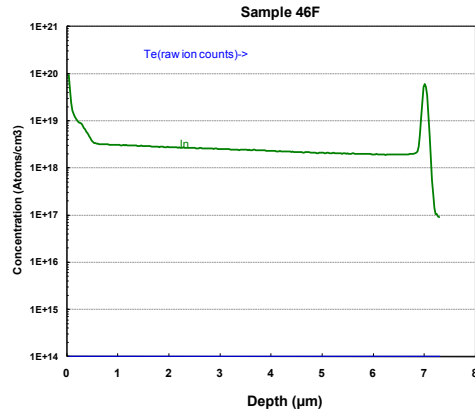
Figure 4. Indium concentration SIMS profile of CdTe on Si sample with indium diffused from the top surface (left) to the back Si interface (right) with an indium concentration of ~ 3x10^{18} cm^{-3}.
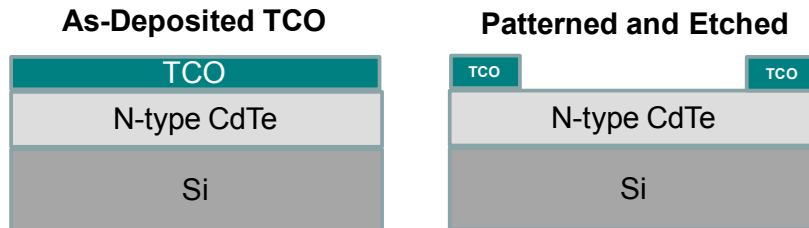
Figure 5. Indium tin oxide was deposited on indium-diffused CdTe by e-beam evaporation. The TCO layers were patterned with photoresist and selectively etched away leaving behind ohmic contact bonding pads that were used for making room temperature Hall measurements.

2.2.2 *Hall Data*
The n-type nature of the indium-diffused CdTe layers was successfully measured using a traditional Hall measurement. Additionally, the ohmic nature of the indium and ITO metal contacts on the n-type surface indicates an n-type conversion. If the CdTe had not converted to n-type, the indium would form a Schottky contact, as indium has a work function of ~ 4.1 eV. Figure 6 illustrates a typical linear ohmic current-voltage (I-V) response between two indium contacts on the surface of n-type CdTe. Table 1 gives an overview of the room-temperature Hall results from the indium-diffused single crystal CdTe on Si samples.
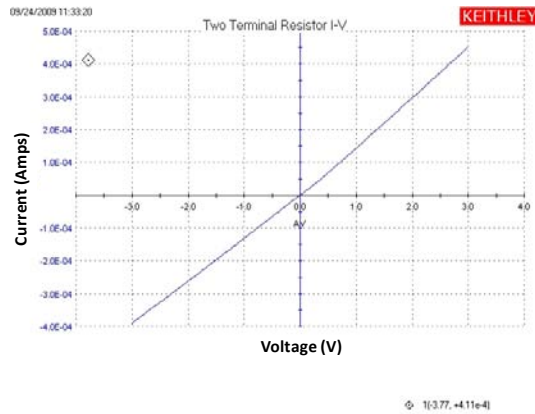
Figure 6. Typical current-voltage (I-V) response between two indium contacts on indium-diffused CdTe illustrating the ohmic nature of the indium contacts.

Table 1. Summary of n-type CdTe Hall Data (~298K).

Sample number	RTP Temperature °C	RTP time (min)	Hall CC (cm^{-3})	mobility (cm^2/Vs)
895-4	400	3	9.6E+17	565
886-1	400	9	3.2E+17	488
886-11	400	9	3.7E+17	365
886-16	425	3	3.6E+17	308
886-10	425	3	2.9E+17	505
886-4	425	3	2.8E+17	492
895-7	425	3	6.7E+17	300
895-8	425	3	4.0E+17	264
887-5	425	3	2.3E+17	537
887-6	425	3	3.8E+17	471
887-7	425	3	4.4E+17	509
895-19	425	9	4.7E+17	453
886-7	450	3	3.4E+17	429
886-8	450	3	2.8E+17	531
886-5	450	9	1.4E+17	523
886-13	450	9	1.5E+17	501

Summary of the Hall Data:

- A consistent $> 10^{17}$ cm^{-3} n-doping with a mobility between 350-550 cm^2/Vs was achieved with our process.

2.2.3 Capacitance-Voltage Measurements of Indium Diffused CdTe

For the C-V samples, indium was deposited as the front n-side contact. The indiffused indium layer forms an n-p$^+$ heterojunction between the n-CdTe and the p$^+$-Si substrate. This structure was used for extracting the n-type carrier concentration using C-V analysis.

The lower doped n-CdTe is depleted during a standard C-V voltage measurement; therefore it is possible to extract the n-type carrier concentration of the CdTe layer from a C-V sweep of the layer. The n-type carrier concentration extracted from the C-V measurement shown in Figure 7 indicates an average n-type doping of $\sim 5 \times 10^{18}$ cm^{-3} over the region probed. This number is qualitatively similar to the indium concentration determined by SIMS for the same sample (46F), suggesting a high level of dopant activation in the CdTe layer. This C-V extracted carrier concentration is also qualitatively similar to the Hall carrier concentration measured for similar samples. The SIMS measurement was performed by Evans Analytical Group (EAG) and verifies that the indium-diffused all the way to the silicon substrate and agrees well with the measured C-V carrier concentration.

Sample 46F
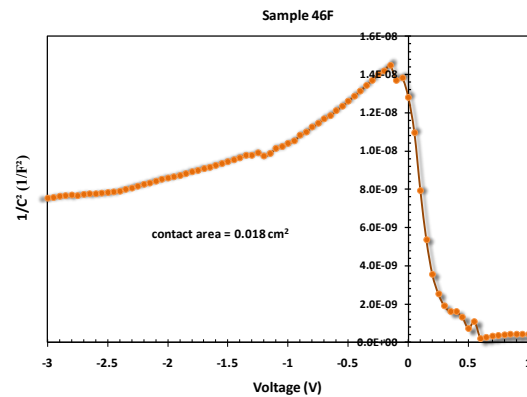
Figure 7. C-V measurement of indium-diffused CdTe. The extracted n-type carrier concentration for this layer is ~ 5x10^{18} cm^{-3}.

2.2.4 Establish CdTe p-type Doping with Carrier Concentration > 3 x 10^{15} cm^{-3}

Multiple approaches were adopted during Q1 to dope the absorber material p-type:

- Post growth Cu diffusion

- Post growth Au diffusion

- *In-situ* As during MBE growth followed by an activation anneal

For either Au or Cu diffusion, a thin layer of Cu or Au was deposited on a CdTe/Si layer and then diffused in by drive-in anneals in an N$_2$ ambient. Schottky diodes were fabricated to extract the p-type carrier concentration from a C-V analysis. Indium was used as the Schottky contact to the p-type CdTe. Approximately 6,000 Å of In was deposited on the CdTe surface to form the Schottky contact. A Cu/Au stack was used as the p-side ohmic contact. Figure 8 (left) and (right) show the plots of the C-V and the extracted active p-type carrier concentrations from representative Cu and Au doped CdTe layers.
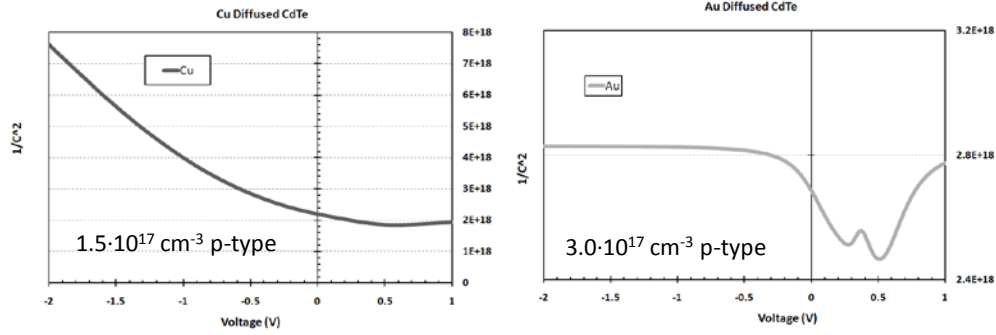
Figure 8. C-V measurement of Cu (left) and Au (right) diffused at 400°C for 10 min in CdTe.

In parallel to the post-growth metal diffusion doping of CdTe, arsenic based *in-situ* doping during MBE growth was also established and is still under development for repeatably reaching higher doping concentrations in the "as-grown" layers. The *in-situ* As_2 doped samples were annealed at 400°C for 30 min in a N_2 atmosphere. A maximum p-type carrier concentration of 7 x 10^{15} cm^{-3} was achieved.

2.3 Develop a Low Resistance Contact to n-type CdTe

During the first quarter of this project, indium tin oxide (ITO) was used as a front contact on the In-doped n-type CdTe. Both sputtering and e-beam evaporation were developed for ITO deposition. Glass slides were used for the development and optimization of the ITO process. Table 2 and Table 3 summarize the performances of the ITOs deposited by sputtering and e-beam evaporation on glass slides.

Table 2. Summary of the ITO Sputtered at EPIR.

Layer	Thickness (Å)	Resistivity x10^{-4} (Ohm-cm)	Transmission > 80% (nm)	Max Transmission
V09051		4	400-1450nm	91% at 450nm
V09051-b	1200	4	400-1500nm	91% at 450nm
V09051-1		5.4		
V09052b	1100	3.6	400-1300nm	91% at 470nm
V09053		78	450-650nm	88% at 500nm
V09053a		6	400-1600nm	90% at 500 nm
V09053-1		3.6	410-1290nm	91% at 470nm
V09053-2	1200	2.8	410-1210nm	90% at 470nm
V09053-3		5.4		90% at 490nm
V09053-4		3.6	410-1310nm	91% at 500nm
V09053-5		3.7	410-1160nm	89% at 470nm
V09054		24	500-840nm	90% at 600nm
V09054a	1500	5	450-1500nm	92% at 570nm
V09054b		5.4		
V09054e		4.5	450-1250nm	91% at 550nm
V09055	2000	18	550-1000nm	90% at 660nm
V09055a		4.8	500-1250nm	91% at 630nm
V09056		6.1	420-1650nm	90% at 470nm
V09056a	1150	4	400-1340nm	91% at 460nm
V09056c		2.5	390-1120nm	90% at 450nm
V09056d		3	390-1230nm	90% at 450nm

Table 3. Summary of e-beam Deposited ITO.

Layer	Thickness (Å)	Resistivity x10^{-4} (Ohm-cm)	Transmission > 80% (nm)	Max Transmission
16-1	~1600	9.2	450-1050	89% @ 600nm
16-3	~1600	8.3	350-1090	89% @ 590nm
16-7	~1600	11	360-1220	91% @ 590nm
16-9	~1600	8.3	350-1100	90% @ 590nm
16-8	~1600	7.7	360-1140	90% @ 590nm

During the e-beam evaporation, the deposited oxide layer loses oxygen due to the energetic nature of the e-beam process. Because of this fact, the e-beam evaporation of ITO is performed in a flowing oxygen environment.

3   Focus of the Second Quarter (Q2)

EPIR's focus during the second quarter was to fulfill the Q2 objectives in the Preincubator proposal and the fabrication of an initial solar cell. The key technology developments targeted during Q2 of the program were as follows:

5. To grow single crystal thin-film CdTe and CdZnTe ((111) and (211)) on p-type doped Si substrates using molecular beam epitaxy (MBE).

6. Achieve top-layer n-type carrier concentration in those CdTe and CdZnTe films with active carrier concentration $> 3 \times 10^{16}$ cm^{-3} and high majority carrier mobility.

7. Achieve absorber p-type carrier concentration $> 3 \times 10^{15}$ cm^{-3} in CdTe and CdZnTe films grown epitaxially on p-type Si substrates.

8. Fabrication of a single-junction CdZnTe solar cell.

3.1   Growth of Thin-Film CdZnTe on Si Substrates with Reasonable Crystallinity Using MBE

The growth conditions required for high quality single-crystal CdZnTe on Si growth are different from the optimal growth conditions for epitaxial single-crystal CdTe on Si. To optimize the growth conditions, a series of growth runs was performed on (111) and (211) oriented Si substrates.

A series of different CdZnTe test structures was grown with different MBE growth conditions including growth-interrupted annealing cycles during the CdZnTe layer growth to relieve the misfit strain of the layer.

The final growth structure is a Cd$_{1-x}$Zn$_x$Te/ZnTe/Si layer structure on p-type Si (see Figure 9). This structure facilitates ease of growth and is useful for single-junction and possible future

multijunction devices. The FWHM of $Cd_{1-x}Zn_xTe$/ZnTe/Si layers is not yet as optimized as that of CdTe/ZnTe/Si layers, however it has the potential to reach similar values.
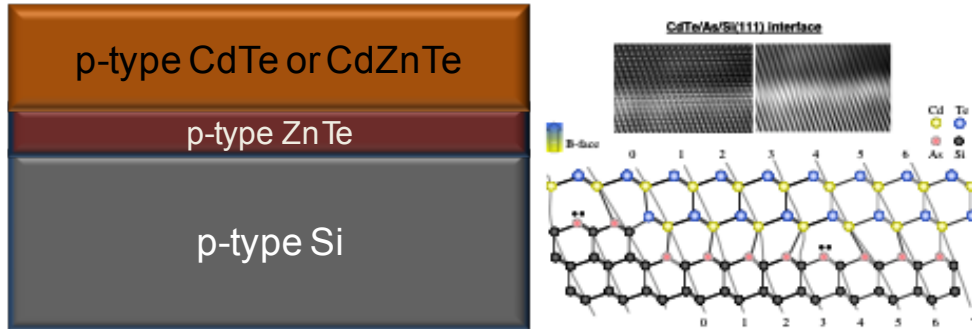
Figure 9. Cartoon cross-section of EPIR's growth stack (left) and cross-sectional TEM images and a stick model of the II-VI/Si interface (right).

The EPIR single-junction device structure uses p-type Si as the back contact, so all device orientated growths were on p-doped low resistivity Si substrates. The growth process and the characterization (wafer image, Nomarski and HRXRD) of the most recent layers are presented here. In all cases, the FWHM of CdZnTe grown on (111) Si is larger than that of CdZnTe grown on (211) Si, an has a correspondingly higher defect concentration. In the best case, the rocking curve FWHM for growth on (111) Si was 2188 arcsec. By HRXRD analysis, the epilayer is tilted $\sim 8°$ away from the surface normal, and both (111) and (211) orientations were detected. However, from the diffracted intensities, the (111) orientation is the dominant orientation.

The layer surface is wavy (see Nomarski image in Figure 10). This surface morphology is a result of the off-axis tilt of the surface and possibly also from an inadequate relaxation of the ZnTe buffer layer prior to the CdZnTe growth.
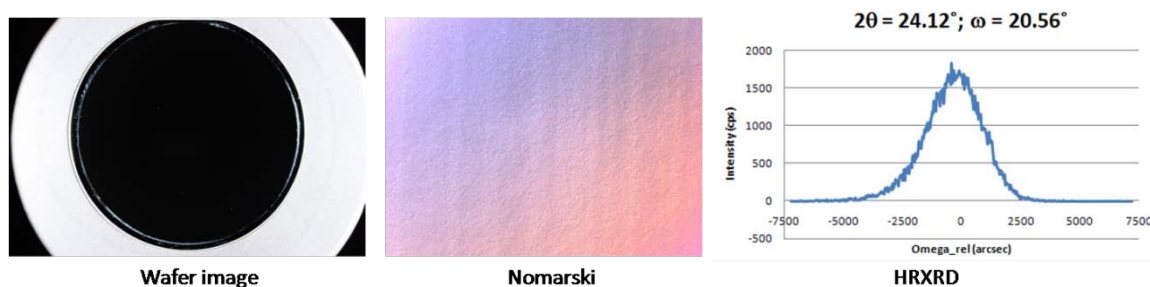
Figure 10. Wafer image, 100x Normarski image of the surface and rocking curve of a recent CdZnTe/ZnTe/Si (111) layer grown at EPIR.

Figure 11 below shows different DCRC FHWM data for recent CdTe and CdZnTe layers grown on (111) and (211) oriented Si substrates. Five layers were grown on n-Si (211) substrates (for

doping control experiments) and the others were grown on p-Si (111) substrates. The highest quality CdTe and CdZnTe to date have been grown on (211) oriented substrates. However, growth optimization should allow for high quality crystal growth on (111) oriented substrates, and in fact CdTe has been grown with a FWHM < 120 arcsec on (111) Si at EPIR. Although it is possible that all future growths will be on (111) Si, the best results to date have been on (211) orientated substrates.
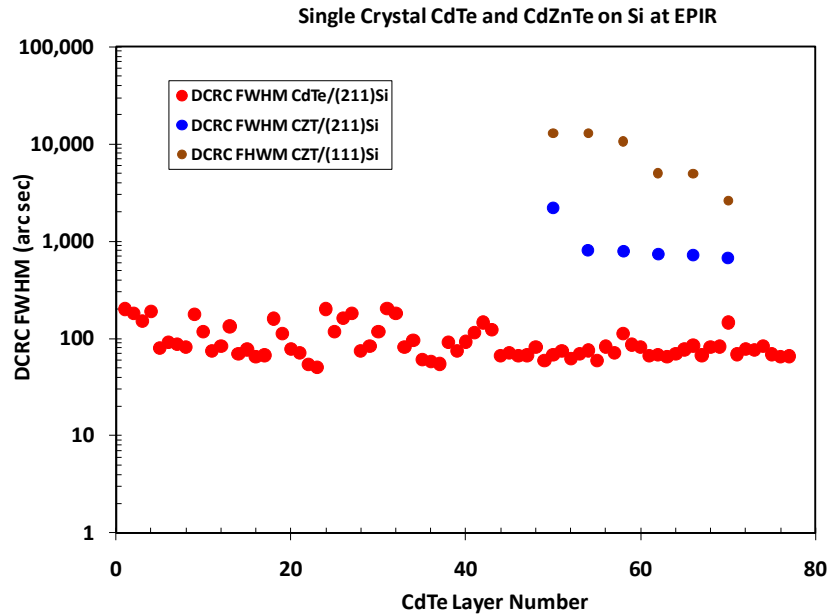
Figure 11. XRD rocking curve FHWM of CdTe and CdZnTe grown on (211) and (111) orientated Si substrates. Growth on (211) provides the for the lowest rocking curve values.

Because of the recent improved results observed in terms of the FWHM and defect densities for CZT grown on Si(211), low resistivity p-type Si(211) substrates (< 0.005 Ohm-cm) are being adopted for future growth of CZT for solar cell development purposes.

3.2   p-type Doping of CdTe

High efficiency II-VI based solar cells require reproducible p-type doping with carrier concentrations $> 5 \times 10^{15}$ cm^{-3} for n-on-p device architectures. CdTe and CdZnTe can be doped in situ during MBE growth with different dopant species. Arsenic is being developed as one possible p-type dopant for single crystal CdTe and CdZnTe single-junction solar cells. An arsenic cracker cell is used to crack As$_4$ to As$_2$ during the growth process. Arsenic is not active as-grown and requires a post-growth annealing process. Different annealing conditions to activate the in situ As-doped CdTe/Si layers were tried. Figure 12 plots the extracted carrier concentration from capacitance – voltage (C-V) measurement for a series of samples with various activation anneals. The arsenic level was measured by SIMS to be approximately 5×10^{16} cm^{-3} for the layers shown in Figure 12.

14
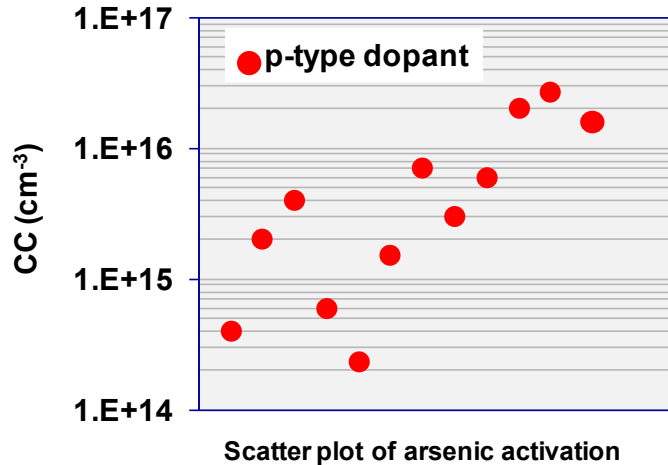
Figure 12. Scatter plot of the measured carrier concentration for sequential samples under various arsenic activation anneals in single crystal CdTe/Si.

Shorter anneals seem to activate As_2 more efficiently than longer anneals. This may be due to the fact that anneals that are too long or performed at too high a temperature create more Te vacancies (donors) than there are As atoms to fill them. These anneals at too high a temperature or too long a duration would increase the ratio of Te vacancies (donors) to Cd and Zn vacancies (acceptors), effectively compensating the p-type As_2 doping. Conversely, a shorter anneal would not result in as many compensating donor V_{Te} sites, and the As_2 concentration would result in a higher effective p-type doping level. A procedure has been developed to establish the reproducibility of the As_2 activation and to establish its value for larger substrates.

Copper and gold have also been explored as p-type dopants. Cu or Au was deposited on clean undoped CdTe/Si substrates, followed by diffusion and activation. Figure 13 is a scatter plot of the measured carrier concentration from recent Cu and Au doping experiments performed on single crystal CdTe/Si.
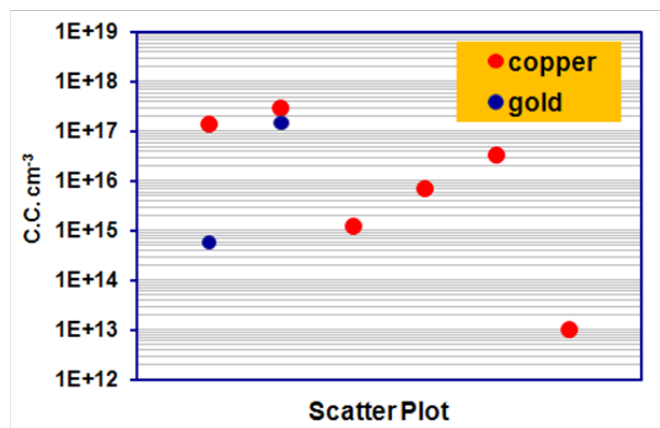
Figure 13. Scatter plot of carrier concentration from recent Cu and Au activation anneals for single crystal CdTe/Si.

3.3   n-type Doping of CdTe

During Q2, EPIR delivered to NREL, as part of the Preincubator Program, indium-doped single-crystal CdTe on a Si substrate. The details of the sample preparation were discussed in the first quarterly report. Figure 14 shows a cross-section of the delivered sample. The single-crystal CdTe/Si sample was doped n-type with indium by indiffusion from the top surface. The indium was deposited by e-beam evaporation onto the sample surface after CdTe (CdZnTe) growth. Indium tin oxide (ITO) contacts were deposited on the four corners of the sample and used as ohmic contacts for Hall measurements.
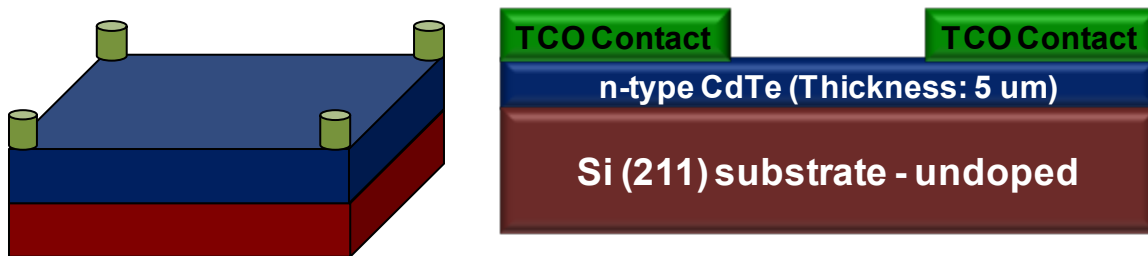
Figure 14. Schematic of indium doped single-crystal CdTe sample delivered to NREL (program deliverable) during the second quarter (Q2).

Figure 15 is a scatter plot of recent room-temperature Hall carrier concentration and mobility data for n-doped single crystal CdTe. EPIR has demonstrated routine n-type doping of single crystal CdTe with carrier concentrations $> 10^{17}$ cm^{-3} and with mobilities greater than 500 cm^2/Vs. Recent annealing improvements have resulted in n-type CdTe Hall mobilities of approximately 1,500 cm^2/Vs including the sample delivered to NREL as part of the Preincubator program.
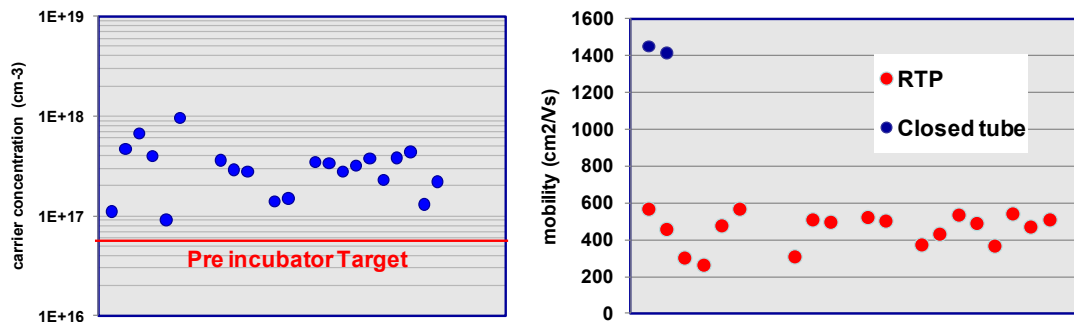
Figure 15. Room temperature Hall carrier concentration (left) and mobility (right) scatter plots of n-type single crystal CdTe/Si samples grown at EPIR illustrating n-type carrier concentrations $> 10^{17}$ cm^{-3} and n-type mobilities greater than 1,000 cm^2/Vs.

3.4   n-type Doping of CdZnTe

During the second quarter, EPIR started working on the n-type doping of CdZnTe with the sample D10025, both single junction and tandem cells will have CdZnTe as the absorber and window layer. Table 4 is a snapshot of our preliminary initial success in doping single crystal CdZnTe/Si using the same approach as used for doping single crystal CdTe/Si.

Table 4. Preliminary n-type doping of single crystal CdZnTe/Si.

Sample	Carrier Concentration (cm^{-3})	Mobility (cm^2/Vs)
25-pp	-7.4E16	1,572
25-ss	-7.8E16	1,500

A detailed study is needed to repeat and reproduce these CdZnTe doping results over a larger number of samples; however, the initial n-type doping results are comparable to the single-crystal CdTe/Si results and are very promising.

3.5   Initial Solar Cell Fabrications

3.5.1   *Junction Depth*

Preliminary EPIR devices were fabricated by diffusing indium in from the top surface of a nominally p-type CdTe or CdZnTe layer to form the n-side emitter in an n-on-p cell architecture. SIMS analysis has been performed on a few of the early cells to determine the emitter thickness (junction depth). Figure 16 is a SIMS plot of the indium dopant level for two developmental solar cells fabricated at EPIR. The junction depths of early cells as measured by SIMS, assuming substantial activation of the indium, were from 1 μm to > 3 μm (see Figure 16). In addition to obtaining consistently high activation, future cell development will focus on reducing the junction depth. This will be achieved by in situ n-type doping, but also could be achieved by reducing the diffusion time or temperature, or by controlled back etching to remove part of the n-doped layer.
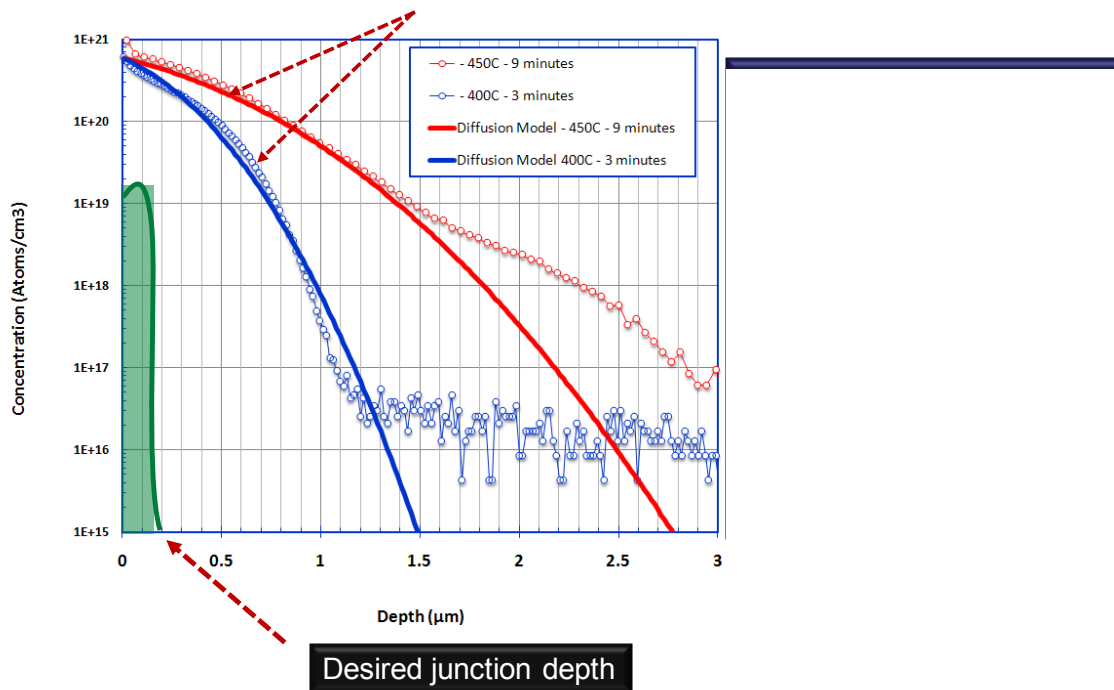
Figure 16. Indium SIMS profile of diffused junctions on EPIR developmental cells indicating a junction depth of several microns (depending on the anneal conditions). The green line represents the ideal junction depth of ~ 200 nm in thickness.

3.5.2 *Short-Circuit Current Density*

The short-circuit current density J_{sc} can be reduced from its ideal value by three effects: (1) the reflection of light at the front surface of a solar cell, (2) the absorption of light in any coating on the front surface, and (3) the recombination of electrons and holes. The third effect also occurs primarily at the front, in the emitter layer, because of the high electron density there, which makes the minority carrier recombination time in the emitter layer extremely small, and because the hole mobilities are much smaller than are electron mobilities. Theoretically, J_{sc} should have been 22 mA/cm^2 for the E_g = 1.8 eV cells and 26 mA/cm^2 for the E_g = 1.66 eV cells. There was relatively little variation in the values of J_{sc} among the different cells we fabricated. For the best cells the value of J_{sc} was ~16 mA/cm^2 for both E_g = 1.8 eV and E_g = 1.66 eV, both with and without an ITO coating. We assume that the ITO both absorbed some incident light and reduced the surface reflection, with the two effects cancelling out, consistent with the measured optical properties of our ITO coatings. From the optical properties of the ITO coatings, we estimate that front-surface reflection and light absorption reduced the possible value of J_{sc} from 22 mA/cm^2 to ~18 mA/cm^2 for E_g = 1.8 eV. Had there been substantial activation of the indium dopants in the very thick emitter layer, almost all electron-hole pairs created in that layer would have failed to contribute to J_{sc}, and its value would have been reduced by more than another factor of two. That was perhaps the first sign that only an extremely small fraction of the indium dopants were activated. The reason for J_{sc} not being larger in the cell with less Zn (a lower bandgap) may be that the indium activation is better with less Zn, which has been observed by others.

18

3.5.3 Fill Factor

A series of cells were fabricated using an indium grid only as the top n-side contact using different indium metal thicknesses. A third contact option using indium tin oxide (ITO) was explored as a method for improving the junction fill factor. Figure 17 is a plot of the experimental cell fill factor for two different cell configurations comparing indium grids of different thicknesses and for an ITO layer used as the top contact. While there is still considerable scatter in the data, the ITO layer dramatically improved the fill factor of the devices, with the best cell fill factors reaching into the mid to upper 70% range, a very promising result.
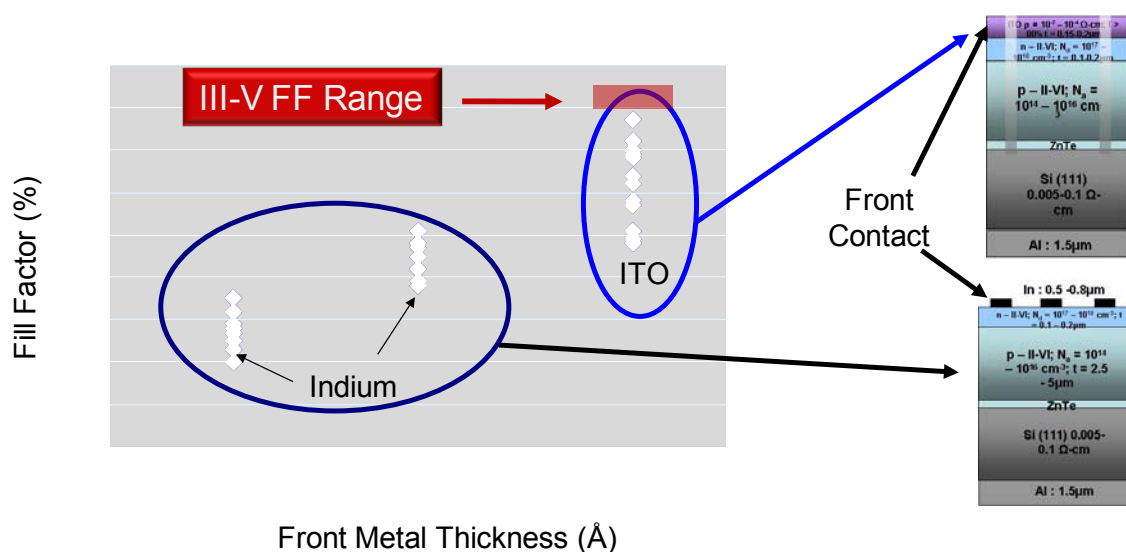
Figure 17. EPIR's single crystal CdZnTe/Si solar cell fill factor for different front contact configurations. The use of ITO as the front side contact has dramatically improved the junction fill factor of our preliminary experimental devices.

3.5.4 Open-Circuit Voltage

The difference between the bandgap of the semiconductor from which a solar cell is fabricated measured in volts, $V_g = E_g/q$ where q is the absolute value of the charge of an electron, and the open-circuit voltage V_{oc} of the cell is an especially important measure of solar cell quality. One cannot obtain state-of-the-art values of $V_g - V_{oc}$ without having both a p-doping level $\geq 10^{17}$ cm^{-3} and minority carrier lifetimes ≥ 50 ns, as shown by Sites and Pan. However, unlike the fill factor and short-circuit current, $V_g - V_{oc}$ is essentially independent of light reflection at the upper surface of the cell and of the front and back contact resistances. We obtained values of $V_g - V_{oc} \approx$ 0.46 V for our best cells, both with $E_g \approx 1.66$ eV and with $E_g \approx 1.80$ eV, approximately equal to the best $V_g - V_{oc}$ values found for c-Si and for III-V materials, and only approximately ~0.04 V above the best value for GaAs. This excellent value of V_{oc} was obtained with $p = 10^{16}$ cm^{-3}; we have since been able to increase p in the absorber region to 10^{17} cm^{-3}, which according to the

calculations of Sites and Pan would increase V_{oc} by 0.06 V and decrease V_g - V_{oc} to 0.40 V, making it even smaller than its value for GaAs.

We first determined the Zn concentrations and bandgaps of the CdZnTe layers from which the solar cells were fabricated. The Zn compositions of the CdZnTe layers were determined by measuring the position of the $2\theta_{mes}$ angle by HRXRD. From the 2θ values of ZnTe (211) and CdTe (211) (76.3866° and 71.2058° respectively), one can find the Zn content of any composition of CdZnTe from

$$[Zn]_{11}(\%) = 100 * \left(1 - \frac{76.3866 - 2\theta_{mes}}{5.1808}\right).$$
(1)

The corresponding equation can be derived for the (111) parameters, leading to

$$[Zn]_{11}(\%) = 100 * \left(1 - \frac{25.2546 - 2\theta_{mes}}{1.4989}\right).$$
(2)

We found $y = 0.278$ and $y = 0.518$ for the two CdZnTe layers from which cells were fabricated Because of the large difference between the lattice constants of CdTe and ZnTe (>5.5%), this determination of the Zn concentration y should be accurate despite the strain in the CdZnTe layers. However, there are substantial differences between the values of E_g given by the three different formulas in the literature for $E_g(y)$ for these concentrations; they give $E_g = 1.66 \pm 0.04$ eV for $y = 0.278$ and $E_g = 1.80 \pm 0.04$ eV for $y = 0.518$. Therefore, we separately measured E_g optically for both layers. As we have spectral response equipment only for the infrared and do not have photoluminescence equipment, we made initial measurements of E_g in-house by reflectivity before sending the cells out for spectral response measurements. We compared specific features in the reflectivity of CdTe and ZnTe near their bandgaps with their known bandgaps, and then used the same relations to determine the bandgaps of the CdZnTe layers from their reflectivities. We again found $E_g = 1.66$ eV for $y = 0.278$ and $E_g = 1.80$ for the two layers. By comparing the accuracy of this same technique for HgCdTe samples with known bandgaps, we estimate the uncertainty in these determinations to be approximately ± 0.02 eV.

3.5.5 Cell Efficiency
The initial cell efficiencies were below 10%, largely due to low fill factors and low short-circuit currents. However, after using an ITO top coating, our best cell, with a 77% fill factor and $V_{oc} = 1.34$, achieved an efficiency of 16.4%, 1.4% above the goal set in our proposal. I-V curves for this cell and for our best cell for $y = 0.278$ are shown in Figure 18. We are confident of being able to consistently repeat the performance of that cell within the next year, and are now engaged in a systematic scientific study to understand all of the physical factors that can affect the performance of a CdZnTe cell. Furthermore, achieving a cell with the same fill factor and open-circuit voltage, but with greatly reduced reflection and absorption of light at the front surface would yield a one-sun single-junction cell with an efficiency of ~22%.
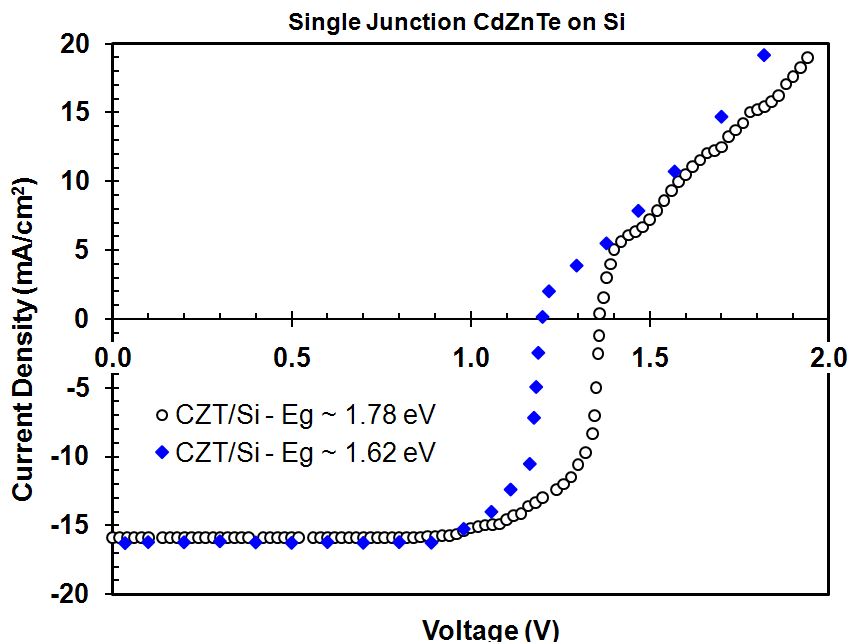
Figure 18. I-V curves under one-sun illumination from our best CdZnTe cells for two Zn concentrations.

4   Focus of the Third Quarter (Q3)

EPIR's focus during the third quarter was to fulfill the Q3 objectives in the Preincubator proposal. The key technology developments targeted during Q3 of the program were as follows:

1. The growth of thin-film CdZnTe on silicon substrates with high crystal quality using molecular beam epitaxy (MBE).

2. Layer stress reduction and the doping of CdZnTe (CZT) n-type.

3. Achieving low resistance ohmic contacts on the p-type absorber layer and consistently achieving p-doping concentrations > 3 x 10^{16} cm^{-3}.

4. Measurement and reduction of the components of the cell series resistance (R_s)

4.1   Growth of Thin-Film CdZnTe on Si Substrates with High Crystal Quality Using MBE

CdZnTe absorber layers have been grown on p-type doped Si substrates with both (111) and (211) orientations (see Figure 19). Two different growth structures were used for solar cell fabrication. One growth structure is a single-layer p-doped CdZnTe absorber layer (Figure 19 left), and the other structure is an in situ grown CdZnTe p-n homojunction with both the p-type and n-type regions being formed during MBE growth. Two different "grown-junction" structures were grown during the past quarter (Figure 19 center and right respectively). The growth parameters of interest are highlighted in Table 5 and Table 6 for (211) and (111) oriented silicon

substrates respectively. In these tables, the layers are classified depending on the growth structure (see Figure 19). The values given in the columns referring to the In concentration are obtained by SIMS in a previous experiment. The In_{cap} column is checked if an indium cap is deposited on top of the stacking at the end of the growth.
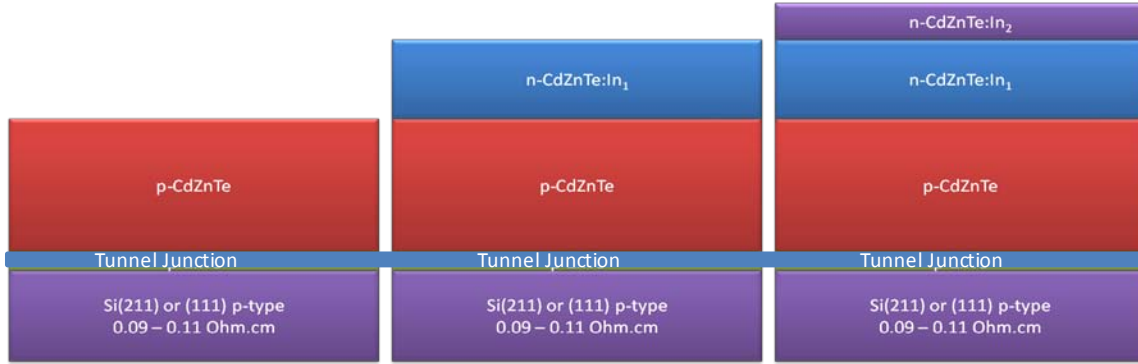
Figure 19. Three different CdZnTe structures grown on Si(111) and Si(211).

Table 5. Growth characteristics of CdZnTe grown on (211) oriented silicon substrates.

ID	p-CdZnTe thickness (um)	In_1 content (at/cm^3)	n-CdZnTe:In_1 thickness (um)	In_2 content (at/cm^3)	n-CdZnTe:In_2 thickness (um)	In_{cap}?
A-type						
D10052	9	-	-	-	-	
D10055 – D10059, D10061	9	-	-	-	-	
D10063 – D10072, D10086	3	-	-	-	-	
B-type						
D10062	9.5	$5\ 10^{17}$	0.5	-	-	
D10073	9.5	$1\ 10^{18}$	0.5	-	-	
D10076	2.5	$1\ 10^{18}$	0.5	-	-	
C-type						
D10077 – D10079	2.5	$1\ 10^{18}$	0.4	$1\ 10^{19}$	0.1	
D10080 – D10081	2.5	$1\ 10^{18}$	0.4	$1\ 10^{19}$	0.1	X
D10082, D10084	2.5	$1\ 10^{18}$	0.4	$5\ 10^{18}$	0.1	X
D10088, D10089	2.5	$5\ 10^{18}$	0.4	$5\ 10^{19}$	0.1	X

Table 6. Growth characteristics of CdZnTe grown on (111) oriented silicon substrates.

ID	p-CdZnTe thickness (um)	In_1 content (at/cm^3)	n-CdZnTe:In_1 thickness (um)	In_2 content (at/cm^3)	n-CdZnTe:In_2 thickness (um)	In_{cap}?
A-type						
D10097	2.5	-	-	-	-	
D10099	2.5	-	-	-	-	
B-type						
D10093, D10095	2	$5\ 10^{19}$	0.5			
D10096	2	$5\ 10^{19}$	0.5			X
C-type						
D10090, D10091	2	$5\ 10^{18}$	0.4	$5\ 10^{19}$	0.1	
D10092	2	$5\ 10^{18}$	0.4	$5\ 10^{19}$	0.1	

The Zn composition of the CdZnTe layer is determined by measuring the position of the $2\theta_{mes}$ angle by HRXRD, as is discussed in Section 3.5.4 above. Table 7 presents the results of the Zn composition for CdZnTe layers grown on (211) oriented Si with a total thickness of 3 microns. The full width at half maximum (FWHM) each layer is also presented. The FWHM values of indium doped and undoped samples are nearly identical meaning that the presence of an In-doped layer in the structure does not significantly influence the crystal quality of the layer. The same conclusion can be drawn for the influence of layer growth rate on the layer FWHM.

Table 7. FWHM, Zn content for 3 µm thick CdZnTe grown on Si(211).

ID	FWHM (arcsec)	Zn fraction (%)
D10065	997.23	37.4
D10067	1022.72	39.0
D10068	974.43	37.0
D10069	988.60	37.4
D10070	1013.68	37.7
D10071	968.01	35.3
D10072	967.78	36.1
D10076	1019.52	38.1
D10077	1008.35	37.8
D10078	1022.33	38.5
D10079	980.09	35.9
D10080	977.18	36.6
D10081	1004.77	37.5
D10084	972.55	36.9
D10088	987.22	34.9

The surface morphology of the as-grown CdZnTe layers was inspected after each growth run. The undoped and indium doped CdZnTe layers look similar (from a surface morphological point-of-view) when the growth substrate is (211) Si (see Figure 20). The surface morphology of layers D10071 and D10088, respectively, shown in Figure 20 represent typical undoped (left) and indium doped (right) samples grown on (211) Si. However, the surface morphology is not the same for as-grown and indium doped CdZnTe layers grown on Si(111) as is shown in Figure 21 (left) (D10097) and (right) (D10093), where the surface morphology of the indium doped sample is seen to be dramatically different from that of the undoped sample.

Figure 20 p-CdZnTe sample D10071 (left) and n-CdZnTe/p-CdZnTe sample D10088 (right) grown on Si(211).
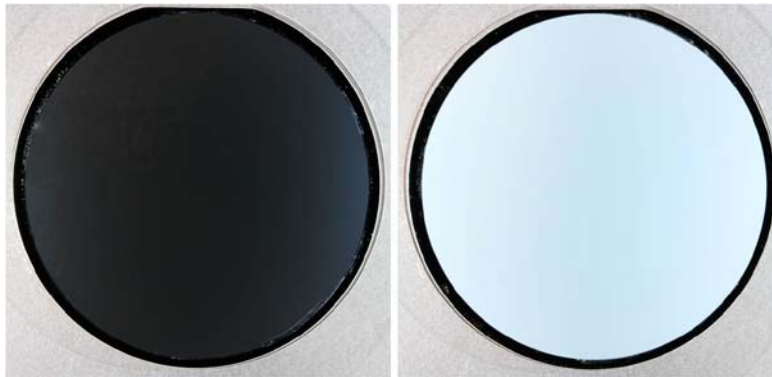
Figure 21. p-CdZnTe sample D10097 (left) and n-CdZnTe/p-CdZnTe sample D10093 (right) grown on Si(111).

The difference between the surface morphology of the two samples grown on (111)Si can be explained by the surface crystal structure. At the end of the growth of n-CdZnTe/p-CdZnTe/Si(211), the RHEED pattern is perfectly 2D whereas it is 3D for the same structure grown on Si(111). Note that for the growth of a single p-CdZnTe layer, the RHEED is 2D at the end of the growth for both substrates.

To determine the impact of the Zn content on the crystal quality of CdZnTe grown on Si, the Zn content for a series of samples grown on (211) oriented Si was intentionally varied between 20%

and 50%. The XRD rocking curve FWHM was measured for each sample and was found to be similar for all layers regardless of the Zn fraction. In the second quarter we demonstrated that a growth rate of about 0.8 µm/hour results in a CdZnTe layer tilted by ~ 10 degrees from the silicon surface for CdZnTe grown on Si(111). These highly tilted layers were not suitable for further device processing. The CdZnTe layers grown on Si(111) that are presented in this report are grown using a growth rate of 0.5 µm/hour. For these growth conditions, no layer tilt was measured relative to the Si substrate.

In summary, we are now able to grow high quality CdZnTe routinely with any Zn composition with a low rocking curve FWHM. We also are able to screen the as-grown wafers for layer stress prior to cell processing.

4.2 Layer Stress and Doping CdZnTe (CZT) n-type

Two techniques were used in the third quarter (Q3) for doping CdZnTe n-type:

1. *In situ* doping using co-evaporation of CdTe, ZnTe and In, in order to create CdZnTe:In n-type layers.

2. Post-growth deposition of an In layer by e-beam evaporation followed by a high-temperature indium diffusion anneal to diffuse the indium into the CdZnTe to dope it n-type.

For *in situ* doped CdZnTe, all of the layers appear normal after growth when inspected under a Nomarski optical microscope. However, after the diffusion of indium into the sample from the sample surface, cracks are sometimes observed when the sample is examined under a Nomarski microscope. The formation of cracks during indium diffusion was found to be independent of layer growth rate, layer Zn fraction over the range investigated, 20% Zn to 50% Zn, and the thickness of the layer. As an example, Figure 22 shows the Nomarski pictures after indium diffusion for two different wafers: (left) D10056, which showed cracks after indium diffusion and layer D10062 (right) that survived indium diffusion without cracking.

Figure 22. Surface morphology of CdZnTe after In diffusion: (left) cracks on sample D10056; (right) no cracks on sample D10062.

From our experiments, we observed that there is a strong correlation between the appearance of cracks after the In diffusion and the spread in the XRD omega scan. The omega scan is a mapping of the angle between the analyzed area and the X-ray beam in the Bragg Brentano geometry. The variation in this angle is a signature of a local curvature of the wafer which can be induced by a strain occurring during layer growth. By dispersion mapping the wafers, it is possible to screen out high stress wafers prior to cell processing. It is also possible to control the growth to eliminate almost all high stress wafers.

4.3 Achieving Low Resistance Ohmic Contacts on the p-type Absorber Layer and Achieving p-type Doping Concentrations > 3 x 10^{16} cm^{-3}

CdZnTe samples with Zn concentrations between 20% and 50% were doped p-type to measure the carrier concentration by Van der-Paw Hall measurements. An undoped high resistive thick CdTe buffer layer was grown in between the Si substrate and the p-type CdZnTe layer to electrically isolate the CdZnTe layer from the Si substrates. Figure 23 is a cartoon cross-sectional schematic of the layer structure used for Hall measurements.
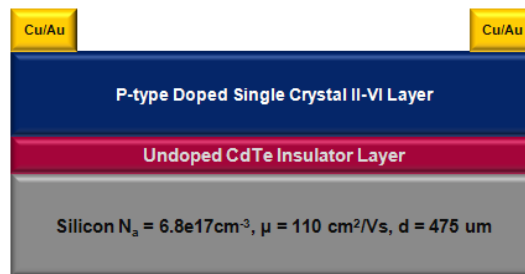
Figure 23. Cartoon schematic of the Hall sample layer structure.

After growth, the samples were diced into 11 x 11 mm^2 pieces. Photolithography was used to pattern contacts at the four corners of each sample. Thin Cu/Au contacts were deposited on the samples to form ohmic contacts to the p-type CdZnTe. Room temperature Hall measurements were performed on the samples and are listed in Table 8. Carrier concentrations in the range of 10^{17} to 10^{19} cm^{-3} and carrier mobilities in the range of 5 – 15 cm^2/Vs were found from the Hall measuements.

Table 8. Hall Data for p-type CdZnTe Layers Grown at EPIR.

Layer	Thickness (um)	avg. growth rate (um/hr)	Zinc content %	defect density cm^{-2}	DCRC FWHM (arcsec)	Hall CC cm^{-3}	Hall u cm^2/Vs
D10053	9.6	0.94	52.2%	8948	682	5.60E+18	9.0
D10056	8.9	0.89	51.1%	7326	672	2.50E+18	12.7
D10058	10.3	0.93	43.6%	11322	600	4.60E+18	5.4
D10061	8.2	0.82	19.2%	12568	525	5.00E+18	10.0
D10062	10.2	0.96	30.6%	46797	550	1.55E+19	5.0
D10067	2.7	0.77	39.0%	456	1022	2.60E+19	6.5
D10068	2.95	0.84	37.0%	887	974	2.20E+19	8.9
D10070	2.9	0.83	35.3%	1705	1013	2.30E+19	6.5
D10073	9.6	0.82	37.4%	17798	634	1.00E+19	2.4
D10074	2.9	0.72	39.6%	2930	1018	3.10E+19	6.8
D10078	3.1	0.83	38.5%	7633	1008	2.90E+19	7.4

Layers D10029 and D10049 (Figure 24) were grown with different p-type dopant levels. Samples from layer 49 were shipped to NREL as part of the Preincubator deliverables. The Hall numbers of layer 49 were later confirmed by NREL.
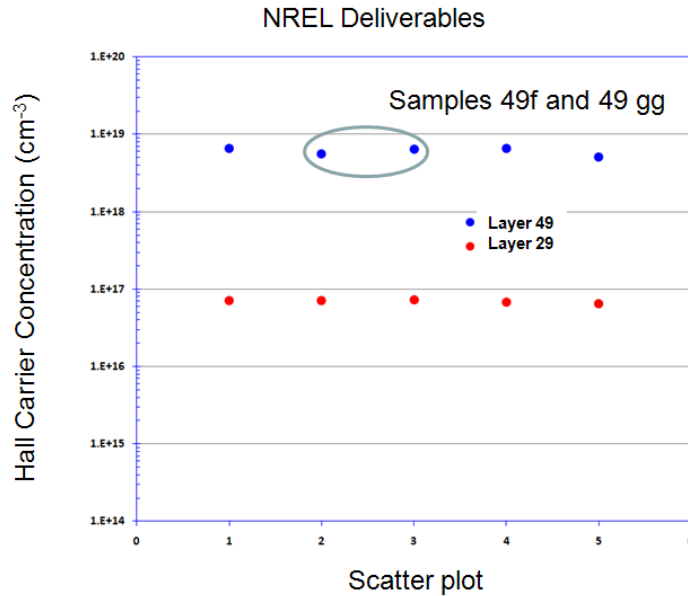
Figure 24. Scatter plot of five different room temperature Hall measurements performed for two different p-type CdZnTe layers. A sample from layer 49 was sent to NREL as one of the Preincubator deliverables.

To confirm that the Zn was not interdiffusing into the CdTe buffer layer, test samples were annealed from layer 49 at higher temperature (400˚C for 30 min in N$_2$). A SIMS analysis of the annealed sample verified that there was almost no interdiffusion of Zn in the CdTe buffer layer from the neighboring CdZnTe and ZnTe layers (Figure 25).
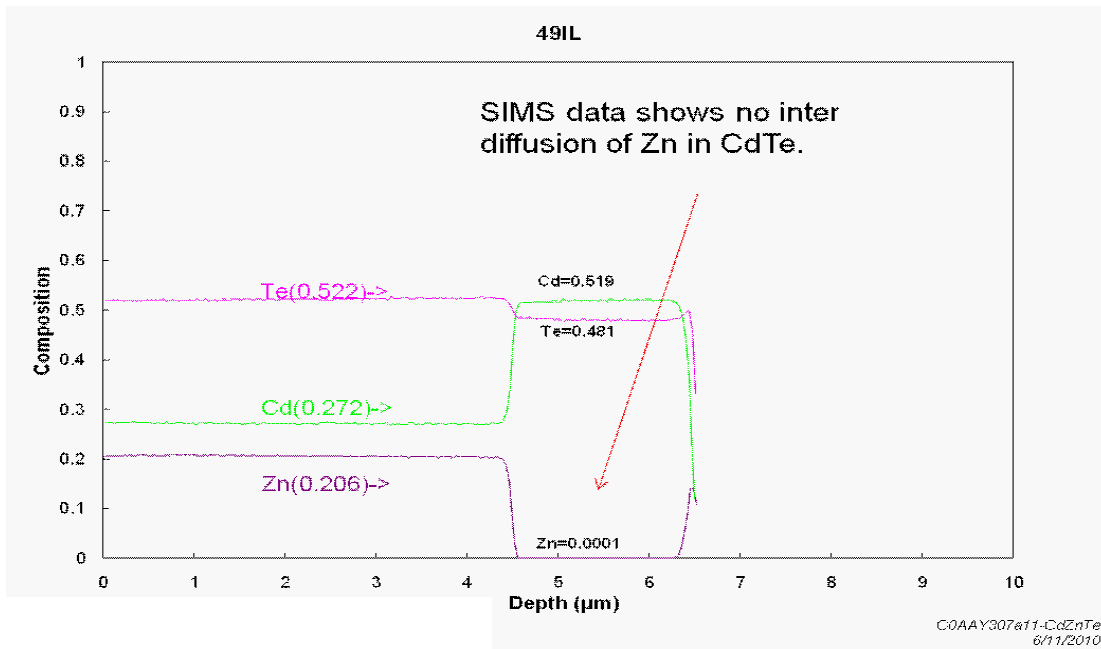
Figure 25. SIMS Zn, Cd and Te profile of the CdZnTe/CdTe/Si layer structure used for Hall illustrating the limited interdiffusion of Zn into the CdTe buffer layer. Courtesy of Evans Analytical Group (EAG).

In summary, we have achieved high levels of p-type doping in CdZnTe samples. We have also demonstrated that the Zn within our wafers is stable under high-temperature anneals.

4.4 Measurement and Reduction of the Components of the Cell Series Resistance (R_s)

Some of the recent cells fabricated at EPIR during the Preincubator program have suffered from a high series resistance (R_s) as measured by the current-voltage (I-V) response of the cell. Figure 26 is a plot of the dark current-voltage (I-V) response of a single crystal CdZnTe/Si cell fabricated at EPIR. A model fit of the I-V curve resulted in a series resistance > 1,000 Ohm·cm^2 and an ideality factor significantly greater than 3 (usually indicating a very high contact resistance). The dynamic resistance area product (R_dA) is plotted as a function of voltage for the same cell in Figure 27, illustrating the high dynamic resistance under a forward bias.

28
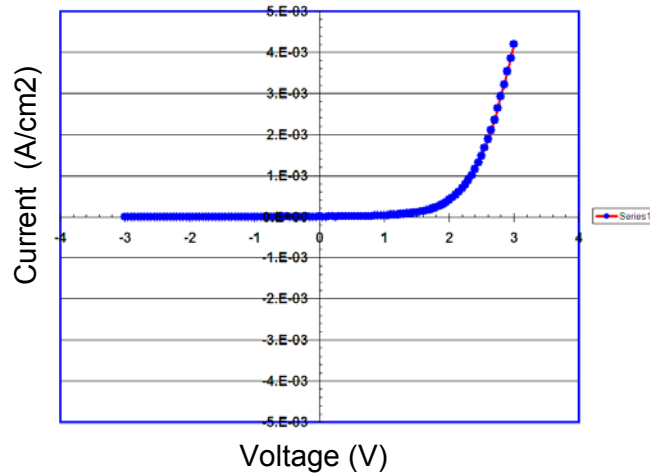
Figure 26. Dark I-V curve of a high series resistance CdZnTe/Si cell with an anomalously high ideality factor.
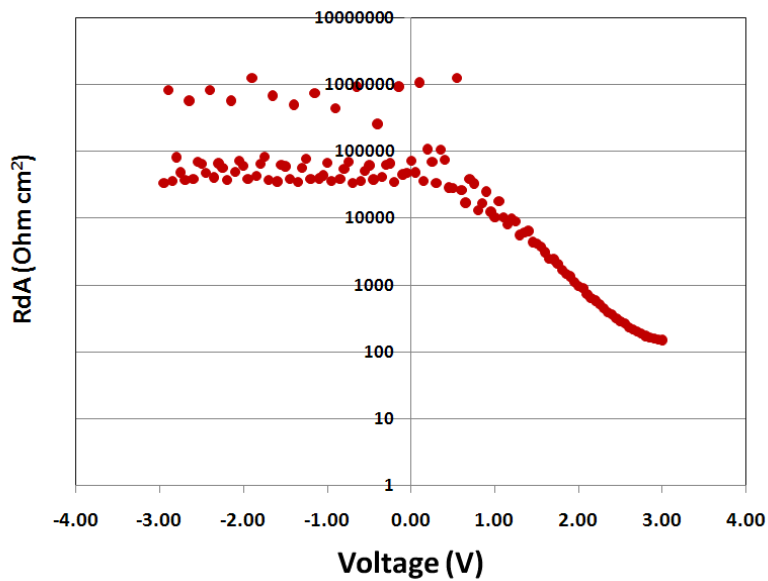
Figure 27. Dynamic resistance-area (R_dA) vs. voltage response of the cell from Figure 28, illustrating the high series resistance as observed in the far forward bias region of the I-V curve.

A series of experiments were performed to isolate the source of the series resistance and eliminate it. Figure 28 shows the cross-section of the EPIR cell structure. The anomalous high series resistance in our cell structure could be from multiple sources, including the front metal/n-CZT interface, the cell emitter, the p-CdZnTe absorber layer, the p-CdZnTe/ZnTe interface, the ZnTe/Si interface, the 500 μm thick p-type Si and/or the back Si/Al contact.
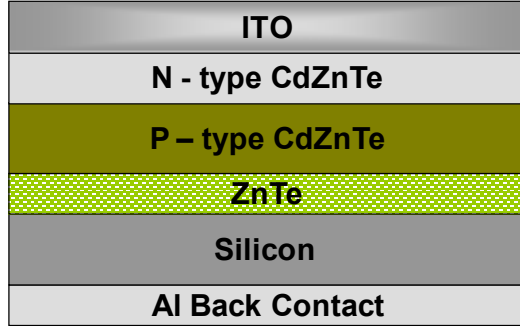
Figure 28. Cross-section schematic of EPIR's single junction device structure.

To determine the origin of the overall cell series resistance, different parts of the cell structure stack were probed independently and the series resistance of each part of the cell stack was compared with the total stack R_s (see Figure 29). The I-V response of the entire cell stack measured in the dark was compared with the dark I-V response of the different cell components. The resistance was determined from the far forward bias characteristics of the current-voltage response. The dynamic resistance-voltage response was derived from the current voltage response and used to determine the series resistance of each component in forward bias (+1 Volt was used as the standard for comparison). It was found that the resistance across the entire stack between contacts 1 and 4 (R_{1-4}) was orders of magnitude higher than when either R_{1-2} or R_{1-3} was measured, indicating that the high series resistance was on the n-side (emitter side) of the junction.
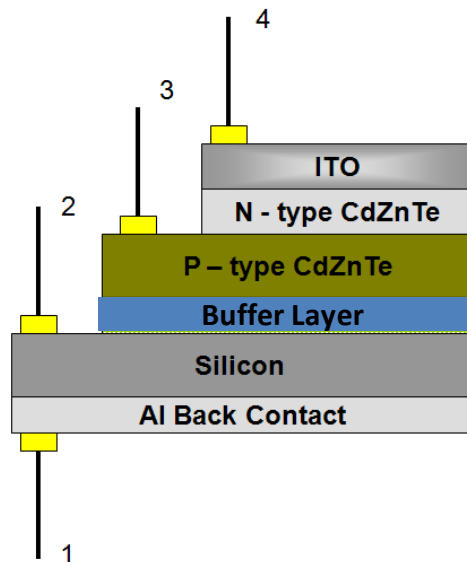
Figure 29. Cartoon schematic of the cell structure with contacts located on different parts of the cell stack that were used to isolate the location of the cell series resistance.

A series of experiments were performed in which a uniform thick indium layer was used as the top contact to the n-side of the solar cell. The thick indium was deposited by e-beam evaporation and annealed to form an ohmic contact to the n-side of the junction. The cell test structure is illustrated in Figure 30.
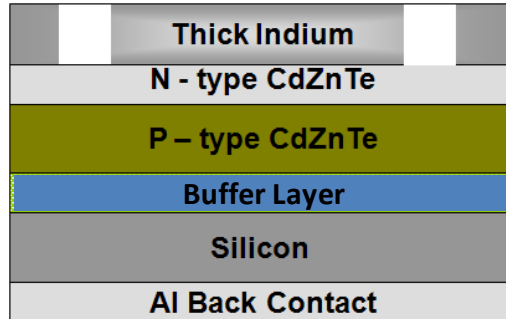
Figure 30. Cross-sectional schematic of the cell test structure used to reduce the series resistance on the n-side of the junction. Thick indium contacts were diffused into the n-side of the CdZnTe in an attempt to form a low resistance n-side contact to the CdZnTe cell. The thick indium is not optically transparent and therefore only dark I-V curves could be measured.

Dark I-V measurements were performed on the test structure illustrated in Figure 30. The dark current voltage response from one of the test cells is plotted in Figure 31. A model fit to the dark I-V is plotted in Figure 32. The model fit to the dark I-V illustrates a dramatically lower series resistance and a junction ideality factor (n) of approximately 1.4. Figure 33 is a plot of the junction R_dA versus voltage response for the same junction. Note the reduced R_dA product at 1 V compared with the R_dA product at 1 V from the cell in Figure 27. This confirms that the high series resistance of the recent cells was due to the n-side contact.
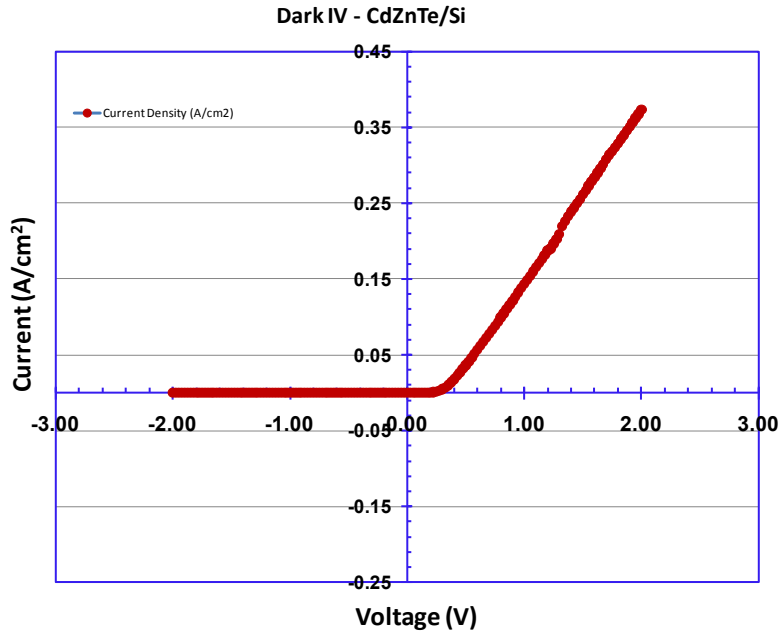
Dark IV - CdZnTe/Si

Figure 31. Dark current-voltage response of a single crystal CdZnTe/Si cell with a solid indium contact on the top surface.

$$I = (Is) \cdot \left[\exp\left[\frac{q \cdot (V - I \cdot Rs)}{n \cdot k \cdot T} \right] - 1 \right] + \frac{V - I \cdot Rs}{Rsh}$$

I-V Curve

R_s = 4 Ohm cm^2

Ideality factor: n = 1.44
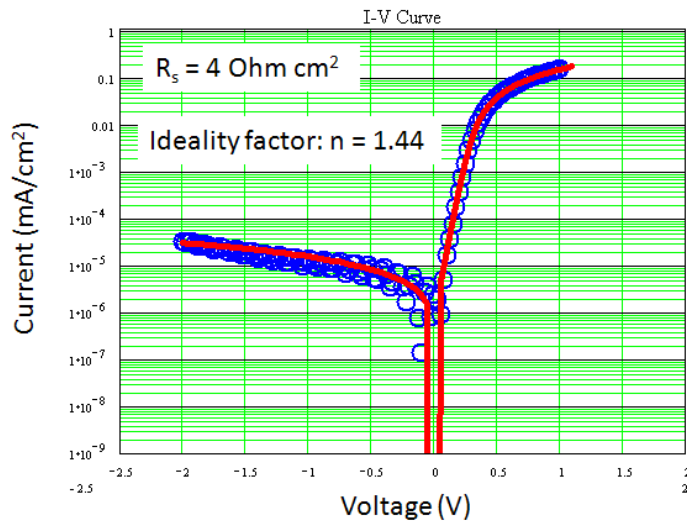
Figure 32. Model fit (red line) to the dark I-V response of a single crystal CdZnTe/Si cell with a solid indium contact on the top surface shown in Figure 31. The junction ideality factor (n) is ~ 1.4 for this cell and the junction series resistance is dramatically lower than that of the cell in Figure 27.

Dark IV - CdZnTe/Si
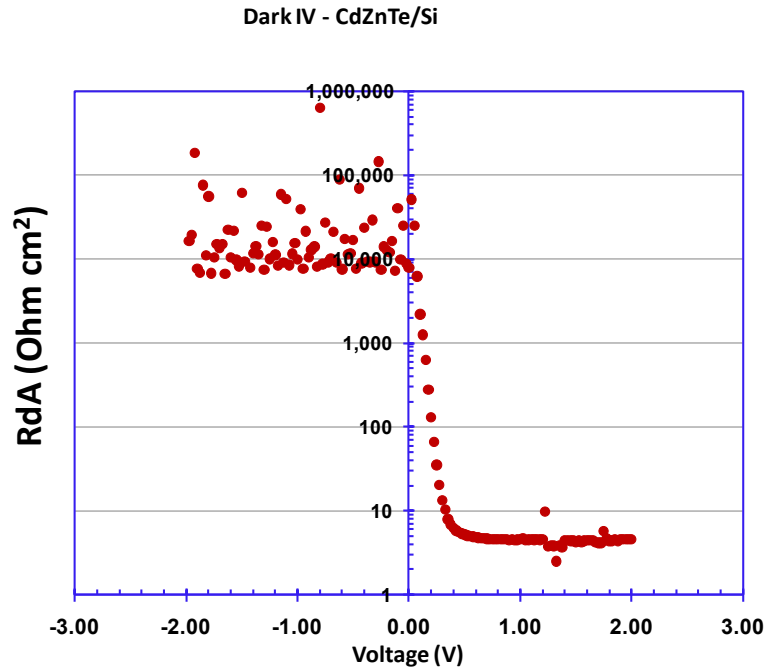
Figure 33. R_dA product vs. cell voltage for the same cell as from Figure 31 and Figure 32. Note that the dynamic resistance at 1 Volt is ~ 4 Ohm cm². This is an orders of magnitude lower resistance than that of the cell in Figure 27.

Additional improvements to the n-side contact have reduced the contact resistance to levels where the total cell series resistance is starting to be dominated by the resistance of the Si substrate. The challenge moving forward is to design an n-side contact metal grid structure that will allow for optical measurements on the cells while preserving the improved n-side contact resistance.

5 Focus of the Fourth Quarter (Q4)

EPIR's focus during the fourth quarter was to fulfill the Q4 objectives in the Preincubator proposal and to systematically study all of the factors that may affect the efficiency of a single-junction CdZnTe solar cell so as to be able to consistently replicate and improve on the results of our best cell discussed in Section 3. The key technology developments targeted during Q4 of the program were as follows:

1. Determination of the bulk minority carrier lifetime τ of unintentionally p-doped CdZnTe grown on Si by MBE and delivery of a sample with $\tau > 100$ ns to NREL
2. N-type iodine doping of CdZnTe

5.1 Determination of the Bulk Minority Carrier Lifetime τ of Unintentionally p-doped CdZnTe (the absorber layer material)

The program goal with respect to minority carrier recombination lifetimes was to achieve lifetimes >100 ns in unintentionally p-doped CdTe/Si or CdZnTe/Si and to deliver a sample with

33

such a lifetime to NREL. The bulk minority carrier lifetime τ of unintentionally p-doped CdTe and CdZnTe was measured at EPIR, NREL and Fisk University by a variety of techniques, with different techniques giving very different results. At EPIR it was measured initially by a contactless microwave method, later by photoconductive decay, and finally by the analysis of the light and dark I-V curves of solar cells. At NREL, the lifetime was measured by time-resolved photoluminescence (TRPL) and photoconductive decay (PCD); and by Arnold Burger at Fisk University, the lifetime was measured by alpha-particle-induced current decay. All measurements were performed on samples with p no greater than $\sim10^{15}$ cm^{-3}, and thus measured the Shockley-Read-Hall lifetime. Auger recombination is negligible in CdTe and CdZnTe epilayers, and the radiative lifetime, $\tau_r \approx 9.4\times10^9$ cm^{-3}s $\times$ (300/T) c^{-1}, is $\sim$9 µs for T = 300 K and $p = 10^{15}$ cm^{-3}.

The EPIR contactless microwave measurements on CdTe gave lifetimes >5 µs. From later measurements it is clear that those measurements did not measure the CdZnTe minority carrier recombination lifetimes; probably they measured trap lifetimes. The EPIR photoconductive decay measurements gave varying results, from <3 ns for samples with unpassivated surfaces up to 1.3 µs for CdTe for the best CdS-passivated CdTe sample and 260 ns for the best CdS-passivated CdZnTe sample (see Figure 36). The results depended strongly on the type and thickness of the passivant because the lateral surface current was being measured, and the surface recombination velocity was very high in the absence of good passivation. Figure 36 shows the photoconductive decay measured by EPIR for the CdTe and CdZnTe layers with the best CdS passivation and with $p \approx 10^{15}$ cm^{-3}.
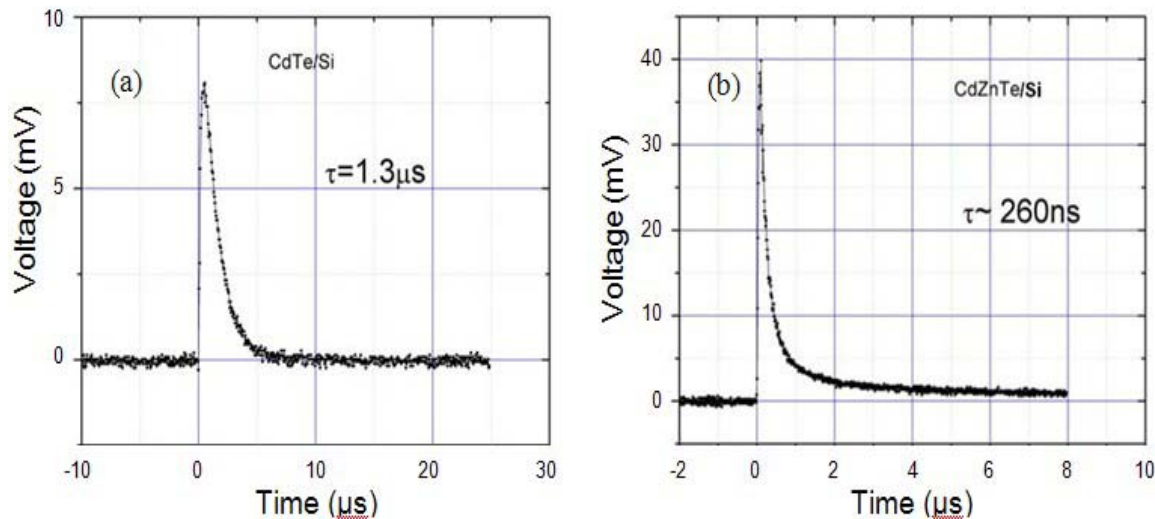
Figure 34. Photoconductive-decay minority carrier lifetimes of unintentionally p-doped (~10^{15} cm^{-3}) CdTe and CdZnTe epitaxial films with the best CdS passivation.

Because the appropriate minority carrier lifetime for the buried absorber region of a solar cell is that of electrons diffusing through the absorber layer toward the top emitter layer, never in contact with the surface, not that of a lateral electron surface current, it will be independent of the effects of surface recombination, and should therefore be longer than that of the electrons moving laterally along the layer surface in a photoconductive decay measurement. Therefore, we

also determined a minority carrier lifetime by analyzing the light and dark I-V curves of some CdZnTe solar cells. The devices had an intrinsic electron concentration $n_i \approx 4 \times 10^5$ cm^{-3}, an acceptor contribution $n_a \approx 10^{14}$ cm^{-3} in the absorber region and a donor concentration $n_d \approx 10^{17}$ cm^{-3} in the emitter region. The fits to the I-V curves of multiple cells yielded lifetimes $\tau > 100$ ns.

A program was written to fit the following equations:

$$J = J_{0Diff}\left(e^{\frac{q(V-R_sJ)}{kT}} - 1\right) + J_{0GR}\left(e^{\frac{q(V-R_sJ)}{2kT}} - 1\right) - J_{Light} - \frac{V - R_sJ}{R_{sh}} ,\tag{3}$$

$$J_{0diff} = qn_i^2 W_d\left[\frac{1}{n\tau_n} + \frac{1}{p\tau_p}\right],\tag{4}$$

and

$$J_{0GR} = \frac{qW_d n_i}{\tau_0}.\tag{5}$$

The generation-recombination current density J_{0GR} and the diffusion current density J_{0diff} were determined from the fittings. In most cases J_{0diff} was negligible, and τ was determined from the equation:

$$\tau_{GR} = \frac{qn_i w_d}{J_{0GR}},\tag{6}$$

with the diffusion length w_d estimated to be 4 µm. The results for three devices are shown in Table 9.

Table 9. Values of the minority carrier lifetime, shunt resistance R_{sh}, generation-recombination current, series resistance and open-circuit voltage obtained from three solar cells.

device	Light	tau (ns)	Rsh	Jogr	Rs	Voc
57Q10	Light	400	1,050	5.6E-11	240	874
61FF	Light	170	1,390	1.4E-10	180	802
61L	Dark	170	280,000	1.4E-10	6,690	n/a
61FF	Dark	160	1E6	1.5E-10	7,600	n/a

The time-resolved photoluminescence measurements performed at NREL gave picosecond lifetimes that are clearly inconsistent with our I-V curves and in particular with the high V_{oc} value found for our best cell. They are not understood, and it has been agreed with NREL that

they may be disregarded. Just as the EPIR photoconductive decay measurements give results that depended strongly on the sample passivation. Although the longest lifetime measured at NREL was only 50 ns, given the extremely strong dependence of the measured lifetime on surface effects, the difference between that result and the >100 ns result found by EPIR on the same sample could arise from differences in the experimental configuration. In any case, it has been agreed that for the reasons discussed above photoconductive decay lifetime measurements do not give results appropriate for considering electron lifetimes in the buried absorber regions of solar cells.

Also, the minority carrier lifetime of a ZnTe passivated undoped single crystal CdTe sample grown on a Si substrate was measured using alpha-particle-induced transient spectroscopy at Fisk University. In this technique, an alpha particle is accelerated towards the CdTe/Si layer stack. The energetic particles excite carriers in the layer stack. A bias voltage that accelerates electrons away from the surface is applied across the sample during the excitation process, minimizing surface recombination effects. The carrier lifetime(s) are extracted from the transient response time of the pre-amplifier signal. The lifetime response of our sample is plotted in Figure 35. Different characteristic lifetimes from the sample including the Si substrate lifetime, the CdTe trap lifetimes and the CdTe minority carrier lifetime can be extracted by analyzing the alpha particle induced carrier decay curve. It is believed that the ~ 25 μs lifetime portion of the curve is from the Si substrates, the ~ 1 and 5 μs decays are typical CdTe trap lifetimes and the 340 ns is the actual minority carrier lifetime of the single crystal CdTe sample. The 340 ns result is consistent with the range of values for τ that we obtained from fitting solar cell I-V curves.

Alpha particles induced transient in ZnTe/CdTe/Si
Alpha particles at anode side, illuminating ZnTe , Bias: 1.4 V

Alpha induced transient
ZnTe/CdTe/Si/CdTe wafer

Slope(1) = .00294
τ_1 = 0.34 μs +/- 4%

Slope(2) = 9.72 x 10^{-4} ns^{-1}
τ_2 = 1.03 μs +/- 3%

Slope(3) = 1.94 x 10^{-4} ns^{-1}
τ_3 = 5.2 μs +/- 2%

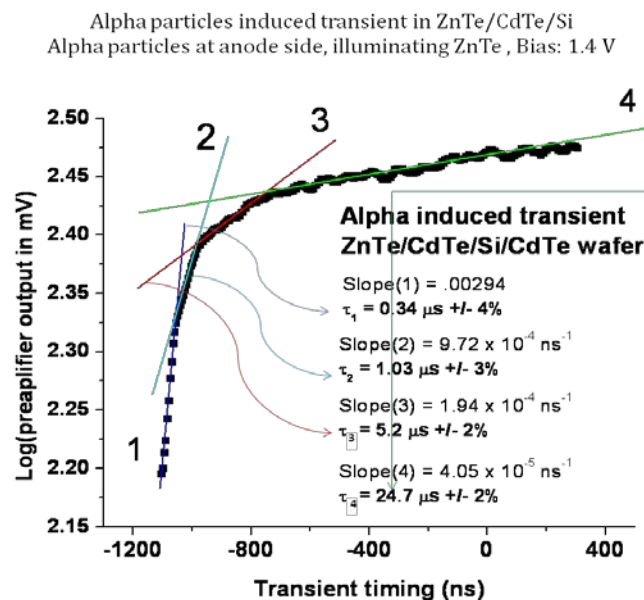Slope(4) = 4.05 x 10^{-5} ns^{-1}
τ_4 = 24.7 μs +/- 2%

Figure 35. Lifetime response of a single crystal CdTe/Si sample measured using alpha particle excitation.

Multiple samples were delivered to NREL for lifetime measurements. The extracted sample lifetimes were very low (in the picosecond range) for time-resolved photoluminescence measurements. This was assumed to be due to rapid absorption of the incident laser beam and subsequent rapid surface recombination effects due to insufficient passivation, rather than a true poor bulk lifetime. Photoconductive decay measurements were then initiated at NREL, again with poor extracted lifetimes. Due to the uncertainty in the lifetime measurement methods, and the large range of extracted lifetimes based upon different measurement techniques, the effort to extract the true bulk lifetime on CZT layers is expected to continue in future joint EPIR and NREL collaboration activities.

5.2   N-type Iodine Doping of CdZnTe

EPIR attached a CdI_2 cell to the Opus MBE chamber, which enabled us to dope CZT layers with iodine to render the material n-type. However multiple attempted iodine n-type activation anneals were unsuccessful. Therefore, it is highly probable that the iodine is incorporated on cation and/or interstitial sites, as is the well-studied case for As p-dopant atoms in HgCdTe. As in HgCdTe, the cation vacancy concentration is orders of magnitude higher than the Te vacancy concentration, so that at the MBE growth temperature much more of the iodine is incorporated on cation sites than on Te sites, despite the lower energy for iodine on Te sites than on cation sites. If that is true, the iodine could be activated by a short anneal at ∼425°C, followed by a longer cation vacancy filling anneal under a Cd and/or Zn overpressure.

As a proposed solution alternative solution, 50 angstroms of indium was sputtered on the surface at an elevated temperature to simultaneously anneal the layer, encapsulate it and indiffuse indium. ITO was immediately sputtered on top of the indium film as a front contact (see Figure 36). Figure 36 shows a schematic of the completed cell structure.
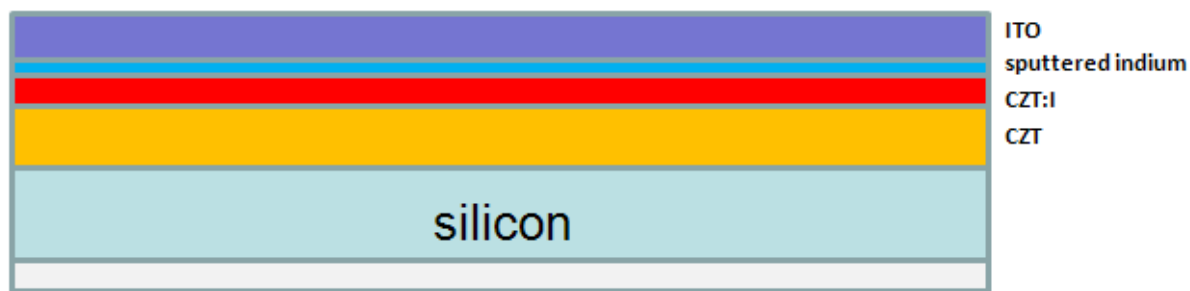
Figure 36. Schematic of the solar cell structure using iodine for doping the emitter layer.

This process produced encouraging results, even though neither in situ iodine incorporation nor indium indiffusion alone produced the desired doping. Although the doping mechanism is still unclear, we conjecture that indiffused indium in the absence of iodine does not displace a significant number of Cd or Zn atoms from cation sites, but that it does displace the iodine from cation sites. If that is true, the resultant n-doping is indium doping with the iodine acting as a catalyst and would allow controlled n-doping with a sharp cutoff controlled by the point at which the MBE iodine incorporation is begun during growth. The iodine SIMS profile and I-V relationship are shown below for layer W10057 in Figure 37 and Figure 38. This is the first

iodine-doped layer that was processed into the device structure shown above. This yielded the best device performance obtained since the original best cell described in Section 3 above, although we have since obtained better cell efficiencies.

Figure 37. SIMS profile of the iodine concentration of layer W10057 in situ doped with iodine. Courtesy of Evans Analytical Group (EAG).
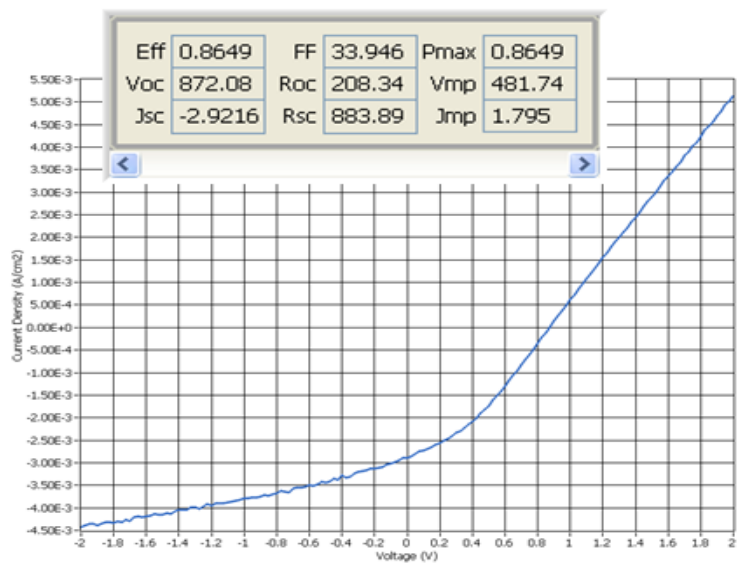
Figure 38. I-V curve from a solar cell fabricated from layer W10057, the iodine profile of which is shown in Figure 37.

Similar processing also was done on layer W10061; this layer had a different iodine profile (see Figure 39), but also produced open circuit voltages > 800 mV. The iodine profile is shown in Figure 39.
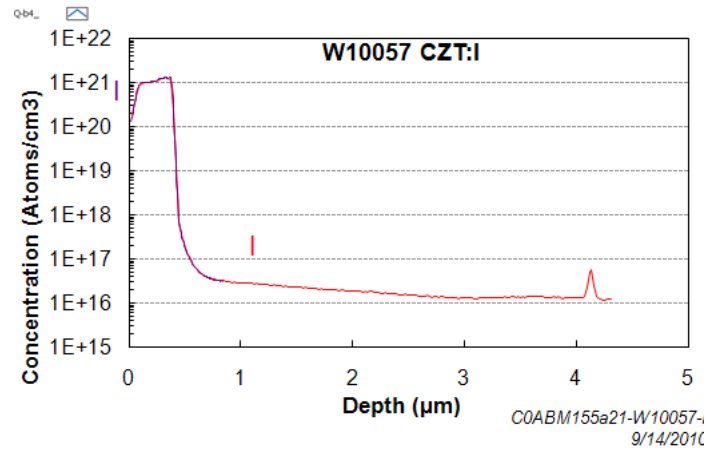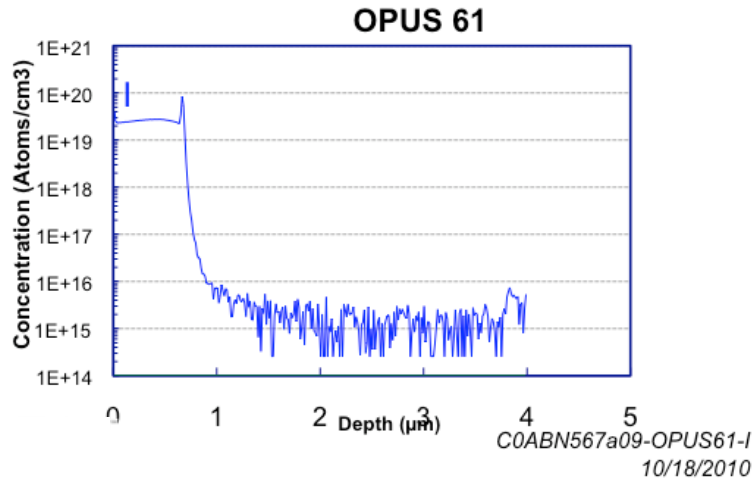
Figure 39. SIMS profile of the iodine concentration of sample W10061 in situ doped with iodine. Courtesy of Evans Analytical Group (EAG).

Figure 40 gives the short-circuit current for cells fabricated from wafers with different dopings and junction depths and the wafer-averages of the short-circuit currents. The current density was found to be approximately inversely proportional to the junction depth, as is expected for very low current densities: this responsiveness to the change in junction depth is encouraging.

Figure 40. The short-circuit current for cells fabricated from wafers with different dopings and junction depths and the wafer-averages of the short-circuit currents.

The performance of the in-situ indium doped layers indicates that it is either the combination of iodine and indium that is boosting cell performance or possibly an MBE-chamber effect. More

experimentation is required to determine what is causing the difference in performance. In particular, measurements of the carrier concentration in the n-doped emitter layer would be very useful.

The characteristics of ten cells fabricated from the additional in situ iodine doped layers, along with the targeted doping profiles, are given in Table 10. The characteristics of eight cells fabricated from the iodine-free in situ indium doped layers, along with the targeted doping profiles are given in Table 11. The I-V curve of the best performing cell, W10074CC, which gave a V_{oc} of 885 mV is shown in Figure 41.
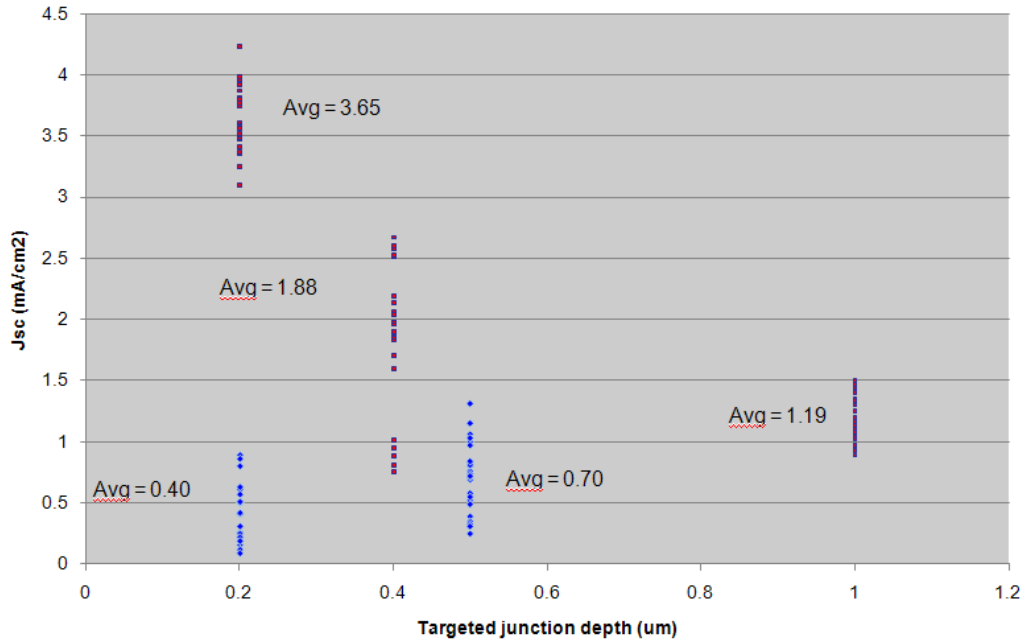
Table 10. Characteristics of ten cells fabricated from the additional in situ iodine doped layers, along with the targeted doping profiles.

sample	iodine doping target (cm^{-3})	Targeted junction depth (um)	Voc	Jsc	FF	Rsh	Rs
74J	1.E+20	0.2	854	3.5	35.4	1032	126
74CC	1.E+20	0.2	858	3.9	39.6	944	68
73U	1.E+18	0.4	769	0.9	30.4	2169	335
73C	1.E+18	0.4	798	1.98	34.7	1545	190
61P	2.E+19	1	850	1.47	42.3	1754	171
61T	2.E+19	1	813	1.07	42.2	2346	185
74X	1.E+20	0.2	852	3.4	33	1254	107
74E	1.E+20	0.2	850	3.8	36.9	958	89
73B	1.E+18	0.4	843	2.5	35	1309	169
61W	2.E+19	1	820	1.1	41.9	1622	190

Table 11. Characteristics of eight cells fabricated from the iodine-free in situ indium doped layers, along with the targeted doping profiles.

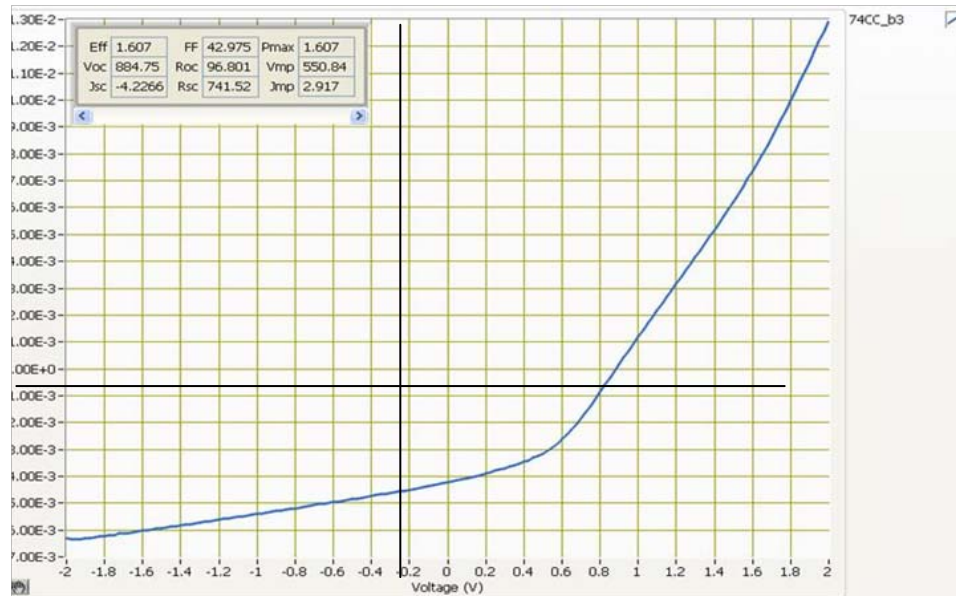| sample	indium doping target (cm⁻³)	junction depth (um)	Voc	Jsc	FF	Rsh	Rs
118E	1.E+20	0.2	636	0.4	29.6	2395	47
118V	1.E+20	0.2	686	0.45	35.4	2875	42
84 O	1.00E+18	0.5	661	0.41	32.5	2635	44
84 R	1.00E+18	0.5	661	0.41	32.5	2635	44
84P	1.00E+18	0.5	622.33	0.57	30	1751.5	54.17
84F	1.00E+18	0.5	698.33	0.72	33.83	2068.33	73.5
118 M	1.E+20	0.2	159	0.51	26.33	781	9.13
118K	1.E+20	0.2	610.6	0.6	29.6	1213.4	13.75

Figure 41. Room temperature, light I-V curve of a cell from sample W10074CC.

6 Program Summary

6.1 Goals and Deliverables

During the course of this program, significant progress was made to further the understanding of the growth, doping and contacting of MBE-grown CdZnTe material and the fabrication of solar cells from that material. The specific goals and deliverables of the program were as follows:

1. MBE growth and delivery of single-crystal epitaxial CdTe/Si with an X-ray double-crystal rocking curve full-width-at-half-maximum (DCRC FWHM) < 200 arcsec and of single-crystal epitaxial CdZnTe/Si with sufficiently good crystallinity for the fabrication of high efficiency solar cells (minority carrier recombination lifetimes 100 ns or longer for unintentionally doped samples),

2. N-type doping and delivery of CdTe/Si or CdZnTe/Si with $n > 3 \times 10^{16}$,

3. P-type doping and delivery of CdTe/Si or CdZnTe/Si with $p > 3 \times 10^{15}$, and

4. Achievement and delivery of an extrinsically p-doped CdTe/Si or CdZnTe/Si sample with a minority carrier lifetime $\tau \geq 100$ ns.

As discussed in detail in the previous sections, each of these program goals was accomplished and delivered on schedule. A CdTe or CdZnTe single-junction solar cell with efficiency $\geq 15\%$, also was achieved. EPIR fabricated a CdZnTe single-junction solar cell with 16.4% efficiency (as measured in-house) from single-crystal CdZnTe with a 1.80 eV bandgap that was grown on Si by MBE. We now are conducting a thorough investigation of the solar cell doping and contacting with the aim of gaining the detailed understanding that will permit us to fabricate high efficiency single-junction solar cells consistently and reproducibly. We expect to be able to consistently fabricate single-junction cells with efficiencies >15% under one sun within the next year and to be able to attain efficiencies >20% under one sun shortly thereafter. The results of this program already represent a tremendous increase in the knowledge base for fabrication of single crystal MBE grown CdZnTe-based solar cells.

6.2 Successes of the Program

Although many challenges remain to be overcome before we are able to consistently fabricate single-junction CdZnTe solar cells with efficiencies >15%, we achieved several notable successes:

1. We demonstrated the consistent MBE growth of CdTe/Si and CdZnTe/Si having high crystalline quality despite very large lattice mismatches.

2. The CdTe/Si and CdZnTe/Si grown consistently showed state-of-the-art electron mobilities and good hole mobilities showing promise of reaching the state of the art.

3. The bulk minority carrier recombination lifetimes of unintentionally p-doped CdTe and CdZnTe grown by MBE on Si were demonstrated to be consistently of order 100 ns or longer, from a factor of three up to an order of magnitude longer than required to obtain a state-of-the-art open-circuit voltage.

4. The desired n- and p-doping levels were achieved.

5. Solar cell series specific resistances <10 Ω-cm^2 were achieved.

6. A single-junction solar cell having a state-of-the-art value of V_{oc} and a 16.4% efficiency was fabricated from CdZnTe having a 1.80 eV bandgap, ideal for the top junction in a tandem cell with a Si bottom junction.

The first three of these successes are especially noteworthy because they mark the achievement of consistent success, which is necessary for product development and commercial success.

6.3 Challenges to Be Met

The primary challenges encountered in this program were with reproducibility. The currently implemented contacting to the n-type emitter is poor and unrepeatable. In particular, the contact between our present ITO and present n-type emitter layers is non-ohmic with a barrier, the specific resistance of our In/n-CdZnTe contacts is high, and we have been unable to deposit a fine closely spaced In grid on the CdZnTe without coalescence of the In.

Although these ongoing challenges are not trivial, progress is being made in overcoming them. Reproducible activation levels are being increased, the contact resistance is being decreased, and these issues will be pursued vigorously under the ongoing collaborative R&D arrangement between EPIR and NREL.

6.4 Outlook for the Future

EPIR expects to be able to overcome the challenges listed above and to be able to consistently produce single-crystal CdZnTe single-junction solar cells with ~22% one-sun efficiencies within the next year and to be able to consistently produce CdZnTe/Si tandem solar cells not long thereafter.

REPORT DOCUMENTATION PAGE

Form Approved
OMB No. 0704-0188

1. REPORT DATE *(DD-MM-YYYY)* May 2011	2. REPORT TYPE Subcontract Report	3. DATES COVERED *(From - To)* 11/19/09 - 1/31/11

4. TITLE AND SUBTITLE High Efficiency Single Crystal CdTe Solar Cells	5a. CONTRACT NUMBER DE-AC36-08-GO28308
	5b. GRANT NUMBER
	5c. PROGRAM ELEMENT NUMBER
6. AUTHOR(S) Michael Carmody and Angelo Gilmore	5d. PROJECT NUMBER NREL/SR-5200-51380
	5e. TASK NUMBER PV10.1199
	5f. WORK UNIT NUMBER

7. PERFORMING ORGANIZATION NAME(S) AND ADDRESS(ES) EPIR Technologies 590 Territorial Dr., Bolingbrook, IL 60440	8. PERFORMING ORGANIZATION REPORT NUMBER NEU-0-99010-12

9. SPONSORING/MONITORING AGENCY NAME(S) AND ADDRESS(ES) National Renewable Energy Laboratory 1617 Cole Blvd. Golden, CO 80401-3393	10. SPONSOR/MONITOR'S ACRONYM(S) NREL
	11. SPONSORING/MONITORING AGENCY REPORT NUMBER NREL/SR-5200-51380

12. DISTRIBUTION AVAILABILITY STATEMENT
National Technical Information Service
U.S. Department of Commerce
5285 Port Royal Road
Springfield, VA 22161

13. SUPPLEMENTARY NOTES
NREL Technical Monitor: Brian Keyes

14. ABSTRACT *(Maximum 200 Words)*
The goal of the program was to develop single crystal CdTe-based top cells grown on Si solar cells as a platform for the subsequent manufacture of high efficiency tandem cells for CPV applications. The keys to both the single junction and the tandem junction cell architectures are the ability to grow high quality single-crystal CdTe and CdZnTe layers on p-type Si substrates, to dope the CdTe and CdZnTe controllably, both n and p-type, and to make low resistance ohmic front and back contacts. EPIR demonstrated the consistent MBE growth of CdTe/Si and CdZnTe/Si having high crystalline quality despite very large lattice mismatches; epitaxial CdTe/Si and CdZnTe/Si consistently showed state-of-the-art electron mobilities and good hole mobilities; bulk minority carrier recombination lifetimes of unintentionally p-doped CdTe and CdZnTe grown by MBE on Si were demonstrated to be consistently of order 100 ns or longer; desired n- and p-doping levels were achieved; solar cell series specific resistances <10 Ω-cm2 were achieved; A single-junction solar cell having a state-of-the-art value of Voc and a unverified 16.4% efficiency was fabricated from CdZnTe having a 1.80 eV bandgap, ideal for the top junction in a tandem cell with a Si bottom junction.

15. SUBJECT TERMS
Photovoltaic; CdTe; Epitaxial; Single Crystal

16. SECURITY CLASSIFICATION OF:			17. LIMITATION OF ABSTRACT	18. NUMBER OF PAGES	19a. NAME OF RESPONSIBLE PERSON
a. REPORT Unclassified	b. ABSTRACT Unclassified	c. THIS PAGE Unclassified	UL		19b. TELEPHONE NUMBER *(Include area code)*

Standard Form 298 (Rev. 8/98)
Prescribed by ANSI Std. Z39.18

F1146-E(10/2008)